Hindawi
Journal of Chemistry
Volume 2024, Article ID 6644815, 19 pages
https://doi.org/10.1155/2024/6644815

Research Article

Novel Phytosomal Formulation of *Emblica officinalis* Extracts with Its *In Vivo* Nootropic Potential in Rats: Optimization and Development by Box-Behnken Design

Varsha Mane,[1,2] **Suresh Killedar**,[3] **Harinath More**,[1] **Sameer Nadaf**,[4] **Sachin Salunkhe**,[5] **and Harshal Tare**[6]

[1]*Department of Pharmaceutical Chemistry, Bharati Vidyapeeth College of Pharmacy, Kolhapur 416013, Maharashtra, India*
[2]*Department of Pharmaceutical Chemistry, Satara College of Pharmacy, Satara 415004, Maharashtra, India*
[3]*Department of Pharmacognosy, Anandi Pharmacy College, Kalambe Tarf Kale, Kolhapur 416205, Maharashtra, India*
[4]*Department of Pharmaceutics, Bharati Vidyapeeth College of Pharmacy, Palus 416310, Maharashtra, India*
[5]*Department of Pharmaceutics, Bharati Vidyapeeth College of Pharmacy, Kolhapur 416013, Maharashtra, India*
[6]*Department of Pharmacognosy, Sharadchandra Pawar College of Pharmacy, Otur, Pune 412409, Maharashtra, India*

Correspondence should be addressed to Varsha Mane; varsha.mane76@gmail.com

Received 2 August 2023; Revised 1 March 2024; Accepted 2 March 2024; Published 4 April 2024

Academic Editor: Maciej Przybyłek

Purpose. The present study aimed to improve the aqueous solubility, permeability, bioavailability, and nootropic potential of standardized *Emblica officinalis* extract (EOE) by developing a novel phytosomal formulation. *Method*. *Emblica officinalis* extract-loaded phytosomes (EOPs) were prepared using solvent evaporation. The EOP was prepared at different molar ratios of extract and phospholipid. Herein, the effects of phospholipid extract ratio (A), temperature (B), and reaction time (C) were systematically investigated on entrapment efficiency using Box-Behnken design. *In vitro* and *in vivo* characterizations of the optimized formulation were performed. *Results*. Optimized EOP formulation ($89.90 \pm 0.24\,\mu$g/ml) exhibited improved aqueous solubility than plain EOE ($11.85 \pm 0.25\,\mu$g/ml). The optimized formulation's particle size and Zeta potential were 198.4 ± 0.20 nm and -39.0 ± 0.40 mv. DSC and XRD studies confirmed the partial amorphization of EOE in phytosomes. Optimized formulation exhibited $69.82 \pm 0.17\%$ of EOE release at 12 h and followed zero-order release kinetics. Moreover, the phytosomal formulation of EOE exhibited its rationality with an improvement of bioavailability by 2.7 folds compared with pure EOE. Compared to EOE, EOP showed significantly ($p < 0.05$) lower escape and transfer latencies on both days in MWMT and EPMT, indicating more effective memory-enhancing activity. Furthermore, EOP-treated rats exhibited improved acetylcholine (Ach) levels than EOE. Brain tissue concentrations measured following EOP oral administration ($1.06 \pm 0.04\,\mu$g/ml) were substantially greater ($p < 0.05$) than those following EOE ($0.32 \pm 0.07\,\mu$g/ml). The brain dopamine and serotonin concentration were found to be higher (16.27 ± 1.209 and 43.28 ± 1.550 ng/ml) in the EOP-treated group as compared to the pure extract-treated group (10.40 ± 1.185 and 32.79 ± 1.738 ng/ml). *Conclusion*. Improvement of aqueous solubility, permeability, dissolution, bioavailability, and narrower particle size distribution could facilitate enhancement in the nootropic potential of EOE phytosomal formulation.

1. Introduction

Memory is the mental capacity for encoding, storing (temporarily or permanently), and recalling past events, thoughts, and sensations when called upon. Less attention, poor memory, slow learning, and weak recall are all visible indications among young and older people in today's stressed and competitive society. Memory loss can lead to forgetfulness, the first sign of cognitive decline [1]. Memory loss that interferes with daily activities could indicate Alzheimer's disease or another dementia.

Neurodegenerative diseases are chronic, debilitating conditions marked by significant cognitive impairment, gradual death of neurons, and secondary abnormalities in

white matter tracts. Large association areas of the cerebral hemispheres of subcortical areas that serve memory and learning are permanently damaged by dementia linked with any illness. It is a condition where one's mental abilities deteriorate when one cannot perform well at work or in social situations. Memory, language, and perceptual problems are all possible symptoms. In addition, impaired motor abilities can make it more difficult for a person to learn essential skills, solve issues, think critically, and make decisions. Dementia can take several forms, including Alzheimer's disease (A.D.), Wernicke–Korsakoff syndrome, and multi-interaction dementia. Alzheimer's dementia strikes people in their middle or late years, accounting for 50%–70% of all cases. Alzheimer's disease is more common as people age, with the prevalence doubling every five years after 65. The three significant structural abnormalities in A.D. victims' brains are the loss of neurons that release acetylcholine, Beta *l* amyloid plaques, and neurofibrillary tangles [2].

Alzheimer's disease and other dementias, such as transient ischemic attacks, stroke, organic brain disorders, mental retardation, and multi-infarct dementia, have few drug treatments available. Therapies are mostly used to treat symptoms right now. There has not been a major therapy breakthrough that prevents, changes, or controls Alzheimer's disease or dementia. The most common AChE inhibitors used to treat cholinergic deficiency in the brain are donepezil, rivastigmine, and galantamine. However, they have problems like a short duration of action, low bioavailability, and a small therapeutic index [3, 4].

Furthermore, several synthetic drugs promoted as cognitive enhancers, such as piracetam, amphetamine, pemoline, pyrithione, and others, are not safe for long-term use in humans due to their additional negative effects and nonspecificity in the site of action. Their use is also limited by serious side effects such as hepatotoxicity. Despite the lengthy development process, only one or two of every 10,000 of these chemical and synthetic compounds are clinically successful and safe enough for regulatory approval in the clinical process. In reality, approximately half of all drug candidates fail clinical trials. Given these significant disadvantages of synthetic molecules, many pharmaceutical companies focus on developing plant-derived drug delivery systems [5].

Herbs and herbal extracts have long been used to treat neurodegenerative diseases. Nootropic herbs and their separated ingredients are called "smart medications" since they act on the brain. Nootropics are called neuro, cognitive, intelligence, and memory boosters. Brain-boosting nootropics come from pharmaceuticals, nutritional supplements, nutraceuticals, or even specially designed-functional meals.

Amla is the Hindi word for the *Euphorbiaceae* plant *Emblica officinalis* fruit, often known as gooseberry. It contains vitamin C, minerals, amino acids, tannin, phenolic compounds, phyllembellic acid, phyllebline, rutin, and emblicol. So far, the literature reveals its use as an antioxidant, antidiabetic, anti-inflammatory, hypolipidemic, antitussive, cardioprotective, analgesic, antiulcerogenic, hepatoprotective, antiatherogenic, antipyretic, and chemopreventive [6].

Although productive and has excellent *in vitro* activity, it does not accomplish or demonstrate the intended *in vivo* effects. This may result from insufficient aqueous solubility, an inappropriate molecular or particle size, or all of these factors, leading to lower absorption and bioavailability [7]. When standardized plant extracts containing phytoconstituents are combined with phospholipids such as phosphatidylcholine, they form phytosomes, herbosomes, or naturosomes, innovative drug delivery technologies. Because of their higher water solubility, these systems have a better absorption profile following oral administration, allowing them to penetrate the biological barrier and boost bioavailability [8]. A more significant concentration of an active component is transported to the site of action when using this phytosome formulation instead of more conventional plant extracts or phytoconstituents. As a result, the therapeutic impact or efficacy is enhanced at low dosages.

Therefore, the current investigation aimed to formulate and characterize the standardized hydroalcoholic *Emblica officinalis* fruit extract (EOE)-loaded phytosomes using the design of experiments (DOEs) approach. Box-Behnken design (BBD) and desirability functions optimized the formulation. The influence of phospholipid: EOE ratio (A), temperature (B), and reaction duration (C) on entrapment efficiency (E.E.) were carefully examined. By producing and testing phytosomal EOE, the quadratic response surface plots were developed to investigate circumstances. The produced phytosomes were physicochemically characterized and tested in rats for memory-enhancing efficacy and pharmacokinetics [2, 9, 10].

2. Materials and Methods

Arjuna Remedies in Kerala, India, provided the standardized hydroalcoholic *Emblica officinalis* fruit extract. VAV Life Sciences Pvt. Ltd., Mumbai, provided LECIVA-S70 (phospholipid). Sigma-Aldrich, Bangalore, provided gallic acid, scopolamine HBr (hydrobromide), and piracetam.

2.1. Preparation of Emblica officinalis Phytosomes. *Emblica officinalis* extract-loaded phytosomes (EOPs) were prepared using a solvent evaporation process with only minor modifications. To make the EOP, several molar ratios of extract and phospholipid were utilized (1 : 1, 1 : 2, and 1 : 3). A round-bottomed flask with a capacity of 250 milliliters was filled with the required amounts of EOE and LECIVA-S70, followed by ethanol (60 ml). According to the Box-Behnken formulation design, the solution was agitated at 700 rpm and refluxed at 40/50/60°C for a fixed time of 1/2/3 h (Table 1). The reflux condenser was attached to RBF and kept on the magnetic stirrer. The resulting solution was vacuum-dried overnight to remove all residues of the solvent. At room temperature, the dried formulation was stored in an amber container until needed [11].

2.2. Experimental Design. This BBD experiment was created using the Design Expert 7.0.0 trial. The BBD approach was used at three levels to see how independent factors affected

Table 1: Factors of the experimental design in each of the three levels areas.

Box-Behnken design (BBD) Independent variables	Coded factors	Levels		
		−1	0	+1
Phospholipid: drug ratio (% w/w)	A	1	2	3
Temperature (°C)	B	40	50	60
Time (h)	C	1	2	3
Dependent variable	Y	Entrapment efficiency in %		

the dependent variable (Table 2). The following is the polynomial equation created by the BDD experiment design:

$$\text{“Y} = \beta 0 + \beta 1\text{A} + \beta 2\text{B} + \beta 3\text{C} + \beta 4\text{AB} + \beta 5\text{BC} + \beta 6\text{AC} + \beta 7\text{A}^2 + \beta 8\text{B}^2 + \beta 9\text{C}^{2\text{”}}. \quad (1)$$

The major, interacting, and quadratic impacts are the independent variables (A, B, and C), (A.B., B.C, and A.C.), and (A2, B2, and C2), where Y is the dependent variable response (here, entrapment efficiency across all levels of factorial interaction combinations), $\beta 0$ is an intercept, and $\beta 1$–$\beta 9$ are regression coefficients from experimental responses against Y values. The labels A.B., BC, and A.C. reflect the change in response when all three parameters are varied concurrently, while A, B, and C are independent variable-coded levels. Independent parameters were chosen after conducting experimental trials and evaluating their impact on E.E. (%). The lowest possible value, the most significant possible value, and the center value were chosen as the three potential levels for the independent variables. Seventeen formulations were developed and characterized for the dependent variable, E.E. (%), according to the indicated experimental design (Tables 1 and 2). The collected data were fitted to the models, and the ANOVA was used to assess them. The second-order polynomial equations were used to explain the models [12, 13].

2.3. Evaluation of Emblica officinalis Phytosome (EOP)

2.3.1. Entrapment Efficiency (E.E.). The E.E. (%) of produced phytosomes was determined using a previously described solvent extraction procedure. In a nutshell, 100 mg of EOP formulation was carefully weighed and distributed in 10 ml of chloroform. The produced phytosomes and LECIVA-S70 were dissolved in chloroform, but EOE remained insoluble. After that, the solution was centrifuged for 20 minutes at 5000 rpm. After removal, the clear supernatant was collected. Then, using a UV/VIS spectrophotometer (U.V. 3000+, LAB INDIA), the nonaggregated EOE was dissolved in ethanol and measured at 275 nm (Remi, Mumbai). Finally, a calibration curve was used to estimate the EOP concentration using $Y = 0.0426x - 0.0072$ regression equation [2].

2.3.2. Particle Size Analysis. Model ZEN 3600, Malvern Instrument, Malvern, U.K., was utilized to measure the particle size of the optimized batch of EOP at 25°C. Water was used to disperse the dispersion. Percentage intensity distribution analyzed complete particle size distribution data down to a few huge particles. In addition, the polydispersity index (PDI) measured size distribution spread [14].

2.3.3. Zeta Potential Determination. The optimized EOP was tested for stability with a zeta potential study. The SZ-100 HORIBA Scientific analyzer was used for the zeta potential analysis (for Windows (Z Type) Ver2.40). The average zeta potential, charge, and mobility of optimized EOP were measured after 60 seconds of analysis [15].

2.3.4. FTIR Spectroscopy. An FTIR-7600 (Lambda Scientific) spectrophotometer was used to get the FTIR spectra of EOE, physical mixture (PM), EOP, and LECIVA-S70. At a pressure of 10 ton/nm^2, a homogenous mixture of each sample (~1 mg) and potassium bromide (~100 mg) was compacted into a disc or pellet. We then scanned the pellet inside the sample container at a resolution of 4 cm^{-1} over the wavelength range of 4000–500 cm^{-1}. FTIR-7600 spectrometer software was used to examine the data.

2.3.5. Powder X-Ray Diffraction Study (PXRD). X-ray spectra of EOE, LECIVA S70, PM, and EOP were recorded using a powder X-ray diffractometer (model: D8 Advance, Bruker AXS, USA) to investigate the polymorphic states of EOE, LECIVA S70, PM, and EOP. The samples were scanned from a setup angle of 0.2–2θ and a count time of 0.5 seconds over a 2θ angle range of 3–60°.

2.3.6. Differential Scanning Calorimetry (DSC). The EOE, LECIVA S70, PM, and EOP were thermally analyzed using a DSC instrument (model: SDT-Q600, TA Instrument, USA). A sealed aluminum pan held a sample size of 4–6 mg. Only one heating cycle was applied to each sample from zero to five hundred degrees Celsius at a rate of ten degrees Celsius per minute. All samples' peaks were analyzed using the device's included software.

2.3.7. Proton Nuclear Magnetic Resonance. The proton nuclear magnetic resonance (^{1}H NMR) spectra of EOE, LECIVA-S70, and EOP were obtained on the ASCEND 500 MHZ BRUKER NMR. At 298 k, all samples were analyzed.

2.3.8. Scanning Electron Microscopy (SEM). The optimized EOP was examined by SEM using SEM equipment (model: JSM-IT 200, JEOL). On the brass stub, carbon tape was applied. The white paper cover was removed on the other

Table 2: Box-Behnken design matrix with actual values and respective entrapment efficiencies.

BBD run	Factor A Phospholipid: drug ratio (%w/w) (drug = 1 gm)	Factor B Temperature (°C)	Factor C Time (h)	Response Entrapment efficiency (%)
1	3	50	1	82.3 ± 1.10
2	2	40	1	80.3 ± 1.60
3	2	50	2	85.8 ± 0.72
4	2	40	3	83.3 ± 0.89
5	2	50	2	85.6 ± 0.93
6	1	50	3	84.3 ± 0.74
7	2	50	2	86.9 ± 0.91
8	1	50	1	80.1 ± 1.30
9	3	40	2	83.2 ± 0.78
10	3	50	3	84.8 ± 0.92
11	1	60	2	87.3 ± 1.23
12	3	60	2	90.3 ± 1.16
13	2	60	1	82.7 ± 0.91
14	2	50	2	86.3 ± 0.88
15	1	40	2	83.6 ± 1.20
16	2	60	3	89.9 ± 1.75
17	2	50	2	86.9 ± 1.98

*The information is shown as mean ± SD values ($n = 3$).

side of the carbon tape. On the other side of the carbon tape, the EOP was sprinkled. Excess samples were retrieved from the carbon tape that had been scattered elsewhere. The brass stub sample was placed in the instrument's main sample container. Scanning electron microscopy with JEOL SEM operation software was used to examine the sample.

2.3.9. Solubility Analysis. An excess of EOE, PM, and EOP was added to 10 ml of n-octanol and water that had been sealed in a glass bottle and kept at room temperature (25°C). An orbital shaker (RIVOTEK) was used to agitate the glass bottles containing the solutions for 24 hours before centrifugation for 20 minutes at 4000 RPM (REMI, India). A membrane filter (0.45 μ) was used to separate and filter the clear super tenant [14–16]. A UV/VIS spectrophotometer (U.V. 3000+, LAB INDIA) was used to evaluate one ml of this clear super tenant after adequate dilutions at 275 nm.

2.3.10. In Vitro Drug Release Study. A dialysis membrane approach was utilized to examine the *in vitro* dissolution of standardized EOE, PM, and EOP. To have dialysis bags ready for the samples, a dialysis membrane (dialysis membrane 60, average flat width −25.27 mm, average diameter −15.9 mm, pore size −2.4 nm, and capacity approximately −1.99 ml/cm, Analab Fine Chemicals) that holds molecules >12,000 KDa was utilized. First, a dialysis membrane was submerged in distilled water for 2 minutes before loading the sample. Next, 50 mg of EOE was dissolved in a 4 ml buffer solution to make an EOE suspension (4 ml). Under the same conditions, an equivalent concentration of EOP was dispersed into a buffer solution. The completed dispersions were then packed in a dialysis bag. Tween 20 (1% w/v) and phosphate buffer saline (200 ml, pH 7.4) were combined in a beaker and then used to suspend the sample-filled dialysis membrane bag floating in the mixture. At 35 ± 1°C, with the magnetic stirrer holding the beaker, we swished the solution and sample-filled dialysis membrane bag at 100 rpm. At regular intervals, 5 ml aliquots of the dissolution medium were taken out and replaced with a new dissolution medium to keep the sink condition the same. The aliquots were filtered via a membrane filter before being examined at 275 nm with a UV/VIS spectrophotometer (U.V. 3000+, LAB INDIA). The aliquots were filtered via a membrane filter (0.45 μ) [16].

2.3.11. Stability Study. According to ICH recommendation Q1A (R2), accelerated stability experiments of the optimized EOP were conducted. The optimized EOP was stored for six months at 40 ± 2°C/75 ± 5% R.H., respectively, in a programmable environmental test chamber (REMI). The samples were taken at 0-, 3-, and 6-month intervals and analyzed for E.E., *in vitro* drug release, particle size, and zeta potential [11, 17].

2.4. Animal Study Protocol Approval. The Institutional Animal Ethical Committee sanctioned the experimental protocol at Crystal Biological Solutions (Crystal Biological Solutions approval no. CRY/2122/070).

2.5. High-Performance Liquid Chromatography (HPLC). Gallic acid was utilized as an identifying marker, and for the marker, a bioanalytical HPLC approach was devised (model: Waters 2695 alliance). A Zorbax SB C18 5 μ (4.6 ∗ 150) mm column was employed in the brain tissue and pharmacokinetic analysis. This experiment was conducted using the chromatographic gradient technique. The mobile phases were water with 0.1 percent formic acid and acetonitrile (ACN) with 0.08 percent formic acid and maintained at

a 1.0 ml/min flow rate. A PDA-style detector was utilized at 271 nm [18, 19] (regression equation: $Y = 67057.54x - 39807$ and retention time: 3.42 minutes).

2.6. A Pharmacokinetic Investigation in the Blood Plasma Compartment. To determine the pharmacokinetics, 18 Wistar albino rats weighing 230–330 gm of both genders were administered (2.3–3.3 ml) 0.5% CMC solution, optimal EOP, and EOE. Following CPCSEA guidelines, Wistar albino rats were maintained in a standard laboratory with unrestricted access to food and water. Animals were fasted overnight until 2 hours after dosage and then fed for the research. The animals were divided into three groups of six. The control group (group I) was given a 0.5% CMC solution (10 ml/kg bw), group II was given EOE (250 mg/kg bw), and group III was given an optimized EOP (equivalent to 250 mg/kg of EOE bw). EOP and EOE were dissolved into a 0.5% CMC solution and administered (2.3–3.3 ml solution) orally to the respective groups. Animal from each group was anesthetized by giving an intramuscular injection of ketamine hydrochloride I.P. Blood samples ranging from 0.5 to 0.7 ml were taken through retro-orbital vein puncture at 0-, 0.5-, 1-, 2-, 3-, 4-, 6-, 8-, 12-, and 24-hour intervals and stored in Eppendorf tubes. Plasma was extracted from all samples by centrifugation at 10,000 rpm for 10 minutes (Remi, Mumbai, India), and the separated plasma was frozen at −40°C for further analysis [16, 17].

2.6.1. Preparation of Plasma Samples for HPLC Analysis. The presence of proteins in the plasma interferes with HPLC analysis of the plasma; hence, there was a need to remove proteins by adopting the protein precipitation method. The centrifuge tube (4 ml) was filled with 2 mL of methanol and 1 mL of separated plasma. The clear supernatant was separated in another tube after 30 seconds of vortexing and 10 minutes of centrifugation at 10,000 rpm. Until HPLC analysis, the protein-free solution tube was frozen at −40°C.

2.6.2. Estimation of Pharmacokinetic Parameters. The HPLC apparatus was loaded with 20 μl of the clear, protein-free supernatant. Based on the peak area measured at various intervals, concentrations were determined. *C* max (maximum plasma concentration), AUC (area under the concentration-time curve), *t* max (time of peak concentration), *t*1/2 (absorption half-life), CL/F (clearance), and V/F (volume of distribution) were all estimated from plasma concentration-time data using a one-compartment extravascular model and P.K. Solver software.

2.7. In Vivo Memory-Enhancing Activity. The memory-enhancing effects of the optimized phytosomal formulation of EOE were measured using the Morris water maze test (MWMT) and elevated plus maze test (EPMT) behavioral models.

2.7.1. Dosing and Sampling Schedule. Thirty-six Wistar albino rats of both sexes, weighing 170–235 grams, were employed in an *in vivo* memory-enhancing activity study. Except for the duration of the experiment, rats had full access to food and water in an animal housing equipped with conventional laboratory conditions.

The animals were divided into six groups of six at random. carboxymethyl cellulose (CMC) 0.5% (10 ml/kg bw) was administered to group I (Control) for 15 days. Scopolamine HBr (0.4 mg/kg bw) was given intraperitoneally (i.p.) into group II (Negative control) on the 15th day. Group III received standard piracetam, 200 mg/kg bw (positive control), orally for 15 days. Group IV: A 250 mg/kg bw EOE dose was given for 15 days, followed by a 45-minute i.p. injection of scopolamine HBr (0.4 mg/kg bw). Group V: the EOP (equivalent to 250 mg/kg bw of EOE) was given orally for 15 days. Then, scopolamine HBr (0.4 mg/kg bw) was delivered intraperitoneally on the 15th day, 45 minutes after the EOP was given. To treat group VI, piracetam (200 mg/kg bw) was given orally for 15 days, and on day 15, scopolamine HBr (0.4 mg/kg bw) was injected intraperitoneally (i.p.) after 45 minutes of piracetam administration.

In 0.5% CMC, EOE, EOP, and piracetam solutions were produced. All the animals were treated per the above-mentioned schedule and subjected to a behavioral analysis study. Simultaneously, the same groups were employed for three different models. The animals were given their pretreatment for the trials using the MWMT, and EPMT, on days that were not consecutive. On day 15, 90 minutes after the relevant dose, the transfer latency (T.L.) and the escape latency (E.L.) were evaluated and compared. After 24 hours had passed since the last treatment, the retention of all learned tasks was assessed. A significant drop in the T.L./E.L. retention value was connected to improved memory [2].

2.7.2. Morris Water Maze Test (MWMT)

(1) MWMT Construction. MWMT was conducted in a 100 cm in diameter and 50 cm in height circular pool. The circular pool had filling and drainage capabilities and was erected on a framework with the water level at waist height. The circular tank's floor was divided into four equal quadrants. Water was added until it reached a depth of 30 cm. In one of the pool quadrants, a 9-cm diameter, the 28-cm-high plastic platform was buried 2 centimeters beneath the water's surface. To make the circular pool opaque, milk was poured. In each trial, the platform was placed in the exact location.

On the first day of the experiment, the rats were trained to swim without a platform. After being deposited into the tank, the animals were given ten seconds to explore the confines of the water and find the secret perch. The rat was given 90 seconds to find the platform; if it still had not done so after that time, it was left for another 10 seconds. On alternate days, rats were trained for 15 days. The trial was successful when the rat sat on the hidden platform within 90 seconds. An error was reported for time spent searching for the concealed platform for more than three minutes.

Throughout the experiment, the platform stayed in the exact location. The E.L. was determined and recorded in MWMT [20].

2.7.3. Elevated plus Maze Test (EPMT). The elevated plus maze was used as a behavioral paradigm to test rats' capacity for learning and memory in exteroceptive conditions. The device's open arms measured 50 by 10 centimeters, while the covered arms measured 50 by 40 by 10 centimeters. The maze was constructed by extending a central platform to a height of 50 centimeters (1 meter). Each rat spent its first day at the end of the open arm, with its back to the central platform. To evaluate the rat's ability to remember where the other sex was hidden, we placed it in one of the compartments. T.L. was determined by timing how long it took a rat on all fours to enter a pair of covered arms holding a rat of the opposite sex. Each animal's T.L. was recorded on day one. Animals were given 90 seconds to enter one of the covered arms before being coaxed or pushed into one. You only have 90 seconds to get your answer in this particular situation. The rat was allowed ten seconds in the maze before returning to its home cage.

2.7.4. Estimation of Acetylcholine (Ach) Esterase Activity in Rat's Brain. On the 16th day, after conducting MWMT, EPMT, and PCT, 5 Wistar rats from each group were anesthetized by giving an intramuscular injection (ketamine hydrochloride I.P.) and decapitated. Rapidly removed brains were cleaned in icy saline and frozen at −80 degrees Celsius for later use. A 0.1 M phosphate buffer (pH 8.0) (0.1 gm of tissue per ml of phosphate buffer) was initially homogenized. Then, 100 μl of DTNB 5, 5-dithio bisphosphate (2-nitrobenzoic acid) and 2.6 ml of buffer were added to a cuvette containing 0.4 ml of homogenate aliquots. The resulting mixture's absorbance at 412 nm was measured in a photometric calorimeter. Once the absorbance had stabilized, a baseline reading was taken, and 20 mL of the substrate (acetylcholine) was added to the solution. The variation in absorbance was monitored every 2 minutes for 10 minutes [21].

2.7.5. Estimation of Dopamine Concentration in Rat's Brain. The rat's dopamine, DA GENLISA™ ELISA kit, was used to quantitatively determine dopamine in Wistar rat brain homogenate solution by sandwich ELISA technique. 50 μl of prepared rat dopamine (DA) standard solutions of 0.3, 0.6, 1.2, 2.4, 4.8, and 9.6 ng/ml were added to respective standard wells. The calibration curve was developed using these reference standards. Each sample well received 40 μl of sample solution comprising homogenized Wistar rat brains from groups I through VI. Each sample well received 10 μl of biotinylated DA antibody. Since the biotinylated DA antibody is already present in the standard solution, it was not included in the standard wells. To each sample well, we added 50 μl of streptavidin-HRP conjugate which combined successfully. After sealing the plate, it was placed in an incubator at 37 degrees Celsius for 60 minutes. After aspirating, washing four times in diluted wash buffer (1X) and blotting the plate upside down with absorbent paper, the plate was finally free of residual buffer. Any residue outside the microtiter wells on the bottom should be wiped up before reading. Each well had 50 μl of TMB substrate A and 50 μl of TMB substrate B poured into it. After covering the plate, we put it in a 37°C oven for 10 minutes. The water in the wells had taken on a bluish hue. Each well had 50 μl of stop solution poured into it. A golden hue replaced the original blue of the wells. Within 10–15 minutes of adding the stop solution, the absorbance was measured at 450 nm using a microplate reader.

2.7.6. Estimation of Serotonin Concentration in Rat's Brain. The rat serotonin, ST GENLISA™ ELISA kit, was used to quantitatively determine serotonin in Wistar rat brain-homogenated solution by the sandwich ELISA technique. The standard wells received 50 μl of serotonin (S.T.) standard solutions at 7.5, 15, 30, 60, 120, and 240 ng/ml concentrations. The calibration curve was developed using these reference standards. Each sample well received 40 μl of sample solution made up of homogenized Wistar rat brains from groups I through VI. Each sample well received 10 μl of biotinylated S.T. antibody. The standard wells did not receive the biotinylated S.T. antibody because it was already present in the standard solution. Each sample well and the standard well received 50 μl of streptavidin-HRP conjugate. In the blank well, the streptavidin-HRP conjugate was left out and mixed well. After sealing the plate, it was placed in an incubator at 37 degrees Celsius for 60 minutes. After aspirating, washing four times in diluted wash buffer (1X), and blotting the plate upside down with absorbent paper, the plate was finally free of residual buffer. Any residue outside the microtiter wells on the bottom should be wiped up before reading. After adding 50 μl of TMB substrate A to each well, 50 μl of TMB substrate B was poured in. After covering the plate, we put it in a 37°C oven for 10 minutes. The water in the wells had taken on a bluish hue. Each well had 50 μl of stop solution poured into it. A golden hue replaced the original blue of the wells. Within 10–15 minutes of adding the stop solution, the absorbance was measured at 450 nm using a microplate reader.

2.8. Procedure for the Estimation of EOE and EOP in Brain Tissue. The concentration of gallic acid in EOE and EOP in brain tissue was determined using a brain-homogenated solution (4 ml) from animal groups IV and V. Two 5 ml centrifuge tubes were filled with the homogenized brain solutions. For 15 minutes, they were spun at 10,000 rpm. EOE and EOP clear supernatants were separated and used for HPLC analysis.

2.9. Histopathological Study. After the treatment session, one animal from each group was anesthetized by giving an intramuscular injection of ketamine hydrochloride I.P., and its brain was dissected. The isolated brains were kept alive in a 10% formalin solution. Next, haematoxylin and eosin

reagents were used to stain the sections and cut them into 3–5 μ thick sections. After placing the brain slices in an optical microscope with a digital camera attached, 400x magnification photos were captured.

3. Results and Discussion

3.1. Preparation of Emblica officinalis Phytosome and Model Investigation. Box-Behnken design matrix with actual values and respective entrapment efficiencies are shown in Table 2. The independent variables' interaction and impact on E.E. were investigated and depicted in a 2D contour plot (Supplementary Figure 1) and a 3D surface response plot (Figure 1). The positive and negative signs in the second-order polynomial equation represented a positive and negative correlation between the components and the resulting response, respectively. The model's significance was indicated by an F value of 30.01, whereas an F value of 0.01 percent probability indicated the presence of noise in the data. Model terms are deemed insignificant if the "probe > F" value exceeds 0.0500. Models A, B, C, AB, BC, and C^2 all have significant terms in our analysis, while models A^2, B^2, and A.C. did not. The model A, B, C, AB, BC, and B^2 variables positively correlate with the response variable, while the terms A.C., A^2, and C^2 negatively correlate. With an F value of 1.77, the lack of a fit was not statistically significant compared to the pure error. Insignificant Fitting in is overrated. The probability of the lack of fit F value being affected by noise due to model leverage is 29.18%. There was little discrepancy between the predicted R-squared value (0.7525) and the corrected R-squared value (0.9423). Our study model showed a signal-to-noise ratio of 19.487, which indicated an adequate signal (Supplementary Table 1). The polynomial equation shows the effect of phospholipid: EOE ratio (A), temperature (B), and time (C) on E.E. (%) as mentioned in the following.

$$\%EE = 86.30 + 0.66A + 2.48B + 2.11C + 0.85AB - 0.43AC + 1.05BC - 0.69A^2 + 0.49B^2 - 2.74C^2. \quad (2)$$

According to the polynomial equation, the independent variables have a positive interaction influence on the response. Therefore, the three independent parameters' optimal values were determined using the preceding information of 3 gm phospholipid to drug ratio, 60°C-reaction temperature, and 3 hours-reaction time, respectively [22, 23]. Detailed results of ANOVA are shown in Table 3.

3.2. Optimized Model Validation. An additional optimized batch of the EOP was made and tested for model validation. The dependent variable, i.e., E.E. (%) of EOP, was determined and compared with that of the predicted value from the model. The validity and practicality of the created model are confirmed by the fact that the entrapment efficiency value (in percentage) of the prepared optimized batch was determined to be 89.15 ± 1.28, which is quite close to the projected value (90.08). Furthermore, using the formula, we could determine that the bias (in percent) was 1.03, which is less than 3%, and hence another evidence of the model's relative robustness [2].

3.3. Particle Size Analysis. The dose and route of administration govern the expected medication particle size for brain and organ deposition. So far, drugs targeting the brain and overcoming the blood-brain barrier have demonstrated that particle size should be within 50–200 nm. It was determined that the optimized EOP formulation had a mean average particle size of 198.4 ± 0.20 nm (Figure 2(a)). Another essential metric is the PDI (polydispersity index), which describes the spread or width of the particle size distribution. Up to a PDI of 0.3 is consistent with the results of lipid-based drug delivery methods like liposome and nanoliposome formulations, indicating a homogeneous population of phospholipid vesicles [24]. The optimized formulation's PDI was found to be 0.238.

3.4. Zeta Potential. The stability of the new formulation can be quantified using the Zeta potential. The optimized formulation's zeta potential was −39.0 ± 0.40 mv (Figure 2(b)). The highly negative zeta potential of −39.0 ± 0.40 mV observed in our formulation can be attributed to the presence of the phospholipid component, particularly LECIVA S70, in the phytosome membrane. LECIVA S70, a commonly used phospholipid in lipidic formulations, contains a polar head group with a negative charge at physiological pH. This negative charge is reflected in the zeta potential measurement of the phytosomes. It is generally accepted that a zeta potential value of more than −30 mv indicates sufficient physical stability. Therefore, a modest zeta potential value, low polydispersity index, and small particle size indicate the new EOP formulation's physical stability [25, 26].

3.5. Fourier Transform Infrared Spectroscopy (FTIR). The FTIR spectra of EOE, LECIVA S70, PM, and EOP are represented in Figure 3. The FTIR spectra of EOE (Figure 3(a)) revealed a characteristic broad and deep band at 3440.39 (broad O-H stretching) and at 2927.41 cm^{-1} (sp3 C-H stretching in alkanes). Peaks indicated the aromatic C=C stretching for the aromatic ring at 1621.84 and 1452.14 cm^{-1}. A few tiny peaks were also found at 1724.05 (C-O stretching), 1342.21 (C-H stretching), and 1189.86 cm^{-1} (C-O stretching).

When analyzing the FTIR spectrum of LECIVA S70 (Figure 3(b)), it is clear that the C-H stretching present in the long-chain fatty acid chain causes peaks at 2925.48 and 2858.06 cm^{-1}. Peaks have also been identified at 1743.33 cm^{-1} (C=O stretching in fatty acids), 1236.15 cm^{-1} (P=O stretching), 1044.44 cm^{-1} (P-O-C stretching), and 970.02 cm^{-1} (-$N^+(CH_2)_3$ stretching). In addition, peaks at 3423.03, 2927.41, 2854.13, 1741, 1641, 1463.71, 1230.36, 1081.66, and 970.02 cm^{-1} were seen in the FTIR spectra of PM (Figure 3(c)), which are indicative of EOE and LECIVA S70 phospholipid. The EOP formulation's FTIR spectra (Figure 3(d)) revealed a broad peak

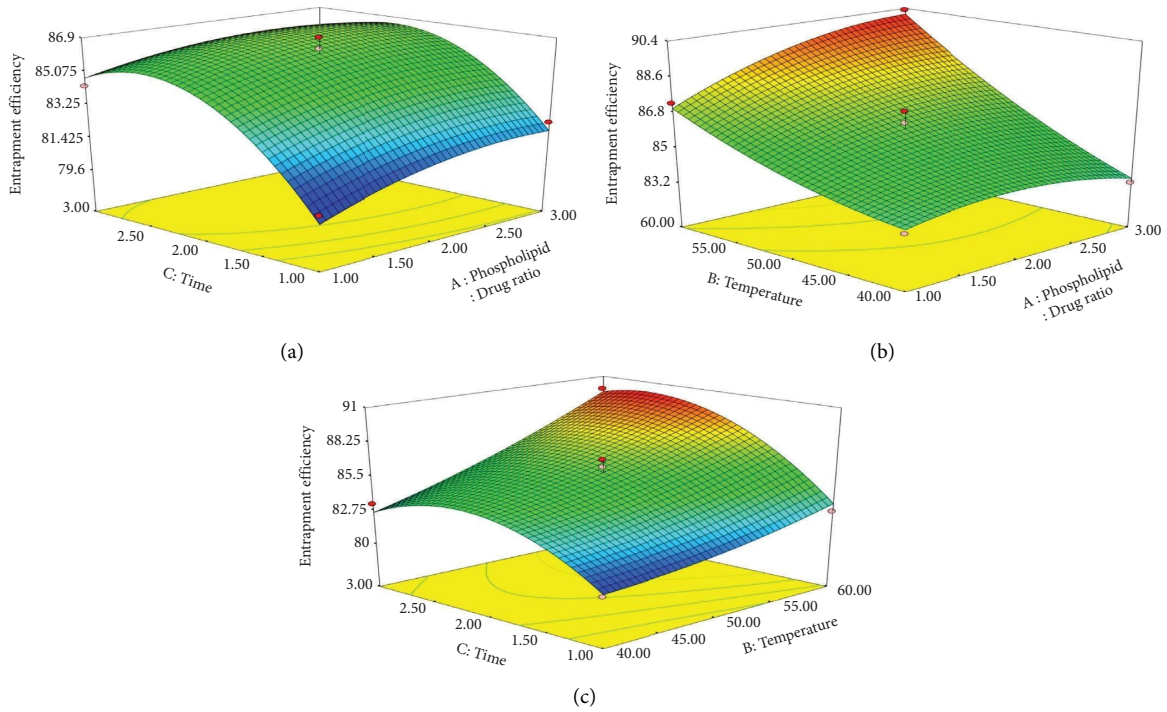

Figure 1: 3D surface response plot showing the interactive effect of (a) phospholipid concentration and time, (b) phospholipid concentration and temperature, and (c) temperature and time on E.E.

Table 3: ANOVA results showing the effect of independent variables on the response studied.

Source	Sum of squares	df	Mean square	F value	p value prob > F	
Model	131.087	9	14.565	30.009	<0.0001	Significant
A: phopholipid: drug ratio	3.511	1	3.511	7.234	0.0311	
B: temperature	49.005	1	49.005	100.967	<0.0001	
C: time	35.701	1	35.701	73.557	<0.0001	
AB	2.89	1	2.89	5.954	0.0447	
AC	0.722	1	0.722	1.489	0.2619	
BC	4.41	1	4.41	9.086	0.0195	
A^2	1.990	1	1.990	4.100	0.0825	
B^2	1.001	1	1.001	2.062	0.1942	
C^2	31.553	1	31.553	65.010	<0.0001	
Residual	3.398	7	0.485			
Lack of fit	1.9375	3	0.646	1.769	0.2918	Nonsignificant
Pure error	1.46	4	0.365			
Cor total	134.484	16				

at 3411.46 (O-H stretch in EOE), 2929.34 (C-H stretch), 1741.41 (C=O stretch), 1463.71 (methylene group bending vibration), 1211.08 (P=O stretch), 1064.51 (P-O-C stretch), and 975.80 cm^{-1}($-N^+(CH_2)_3$ stretch).

The FTIR spectra of EOP with EOE and phospholipid LECIVA S70 showed changes in specific EOE regions due to EOE interaction with LECIVA S 70. The O-H stretching frequency of EOE at 3440.39 cm^{-1} changed to 3411.4 cm^{-1} in the EOP, indicating the presence of weak intermolecular interaction during the formation of EOP. In the EOE FTIR spectra, a very weak negligible peak appeared at 1724.50 cm^{-1} but appeared a strong signal in the EOP at 1741.41 cm^{-1}. The EOE peaks at 1189.86, 1110.80, and 1033.66 cm^{-1} had vanished as had the development of two LECIVA S70 phospholipid peaks with minor frequency shifts in EOP. Changes in peak wavenumber of LECIVA S70 at 1236.15 and 1093.44 to 1222.08 and 1084.51 cm^{-1}, respectively, in the EOP also represented the presence of weak intermolecular interaction between EOE and LECIVA S70 phospholipid [27].

3.6. X-Ray Diffraction. Figure 4 shows the EOE, PM, LECIVA S70, and EOP X-ray overlay diffraction peaks. EOE's diffraction peaks (Figure 4(a)) exhibited multiple intense and sharp peaks, indicating that it is crystalline. Crystallinity peaks were detected in EOE at 2θ values of

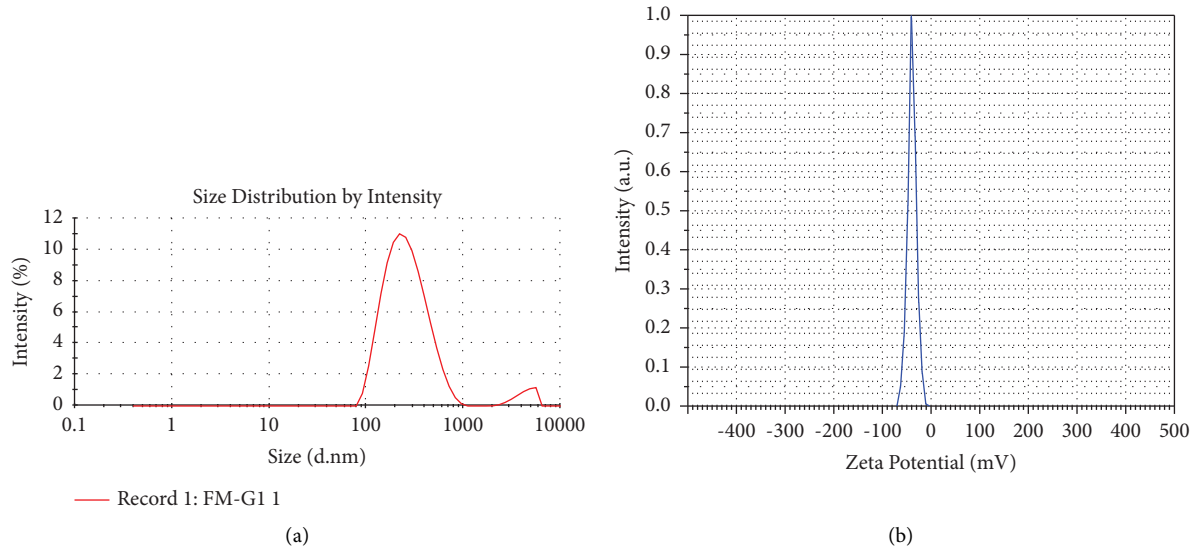

Figure 2: (a) Particle size distribution and (b) Zeta potential of optimized EOP.

12.60, 19.69, 23.37, 28.37, 31.16, 34.78, and 37.94°. Phospholipid LECIVA S70 (Figure 4(d)) exhibited three peaks; two were small and relatively broad, at 2θ values of 5.6, 7.5, and 20.27°, respectively. The physical mixture (PM) diffractogram (Figure 4(c)) presented a few crystalline peaks with lower intensity than EOE and two associated with LECIVA S70 at 2θ values of 7.54, 19.72, 26.16, and 28.25°.

The reduced amount of EOE in the sample, *in situ*, creation of partial aggregates between EOE and LECIVA S70, or interference by the LECIVA S70 molecule generating partial amorphization of EOE could all explain the drop in crystalline peak intensity. The diffraction pattern of EOP (Figure 4(b)) revealed peaks at 2θ values of 12.57 and 21.04°. Distinct crystalline peaks seen in the diffraction pattern of EOE were almost absent in that of EOP. Amorphization of the EOE phospholipid complex is evidenced by the disappearance of nearly all of the crystalline peaks present in EOE. EOE in the LECIVA S70 matrix may exist in a molecularly distributed or amorphous state, according to the EOP diffraction pattern [28].

3.7. Differential Scanning Calorimetry. EOE, LECIVA S70, PM, and EOP's DSC thermograms are displayed in Figure 5. EOE's thermogram revealed a prominent endothermic peak at roughly 105°C (Figure 5(a)). The thermogram of LECIVA S70 (Figure 5(b)) showed two sharp peaks. At 135.27°C, the first peak occurred, most likely caused by phospholipid melting. The second peak appeared at 297.35°C, indicating that the phospholipid hydrocarbon segment had undergone isomeric or crystal changes during the transition from the gel to the liquid crystalline state [29]. Two peaks appeared in the PM thermogram (Figure 5(d)) at 112.5°C and 135.27°C. It is possible that as the temperature rises, the phospholipid melts and the EOE dissolves in it, indicating the partial production of phytosomes. The thermogram of EOP (Figure 5(c)) revealed one new broad endothermic peak at 90.20°C, while the EOE and LECIVA S70 peaks were absent. The medications' higher solubility and lower crystallinity may account for decreased melting point and enthalpy [22]. The presence of weak intermolecular interactions, such as van der Waals interactions and hydrogen bonding, between EOE and LECIVA S70 during the formation of the drug-phospholipid complex is consistent with the fading of the initial peak of EOE and LECIVA S70 on the EOP thermogram and the lower value of phase transition temperature than LECIVA S70. The absence of LECIVA S70's second endothermic peak as the phase transition temperature drops could be attributable to a progressive decline in the phospholipid hydrocarbon chain. The decrease in the phospholipid hydrocarbon chain is responsible for establishing a connection between EOE and the polar area of the phospholipid, followed by EOE entrapment with long-chain hydrocarbon tail phospholipid molecules [30].

3.8. Proton Nuclear Magnetic Resonance. ^{1}H NMR of EOE, LECIVA S70, and EOP are shown in Figure 6. ^{1}H NMR of EOE (Figure 6(a)) exhibited the following peaks: δ 3.756 (33H, s), δ 4.199 (22H, s), δ 6.912 (21H, s), δ 7.074 (2H, s), and δ 7.377 (9H, s). ^{1}H NMR of LECIVA S70 (Figure 6(b)) showing the following peaks: δ 0.855 (7H, d), δ 1.232–1.255 (44H, d), δ 1.494–1.507 (5H, s), δ 1.990–2.018 (9H, d), δ 2.257–2.271 (5H, d), δ 2.730 (3H, s), δ 3.124 (8H, s), δ 3.444 (3H, s), δ 3.495 (2H, s), δ 3.504–3.527 (3H, s), δ 4.302–4.776 (3H, s), and δ 5.308–5.320 (8H, d). ^{1}H NMR of EOP (Figure 6(c)) showing following peaks: δ 0.854 (6H, d), δ 1.235–1.258 (35H, d), δ 1.493 (4H, s), δ 2.004–2.031 (7H, m), δ 2.256–2.285 (3H, m), δ 2.363 (1H, s), δ 2.633–2.637 (1H, s), δ 2.717–2.729 (3H, d), δ 3.123 (9H, d), δ 3.342 (4H, s), δ 3.404 (4H, s), δ 3.444 (3H, s), δ 4.190 (3H, s), δ 5.307–5.334 (7H, m), and δ 6.911(1H, s).

When the ^{1}H NMR graphs of EOE and EOP were compared, differences in the upfield (<3) and downfield (>3) were discovered. The development of phytosomes was indicated by a shift in the proton signals in the area of the ^{1}H NMR of EOE and EOP (>3). Furthermore, the presence of

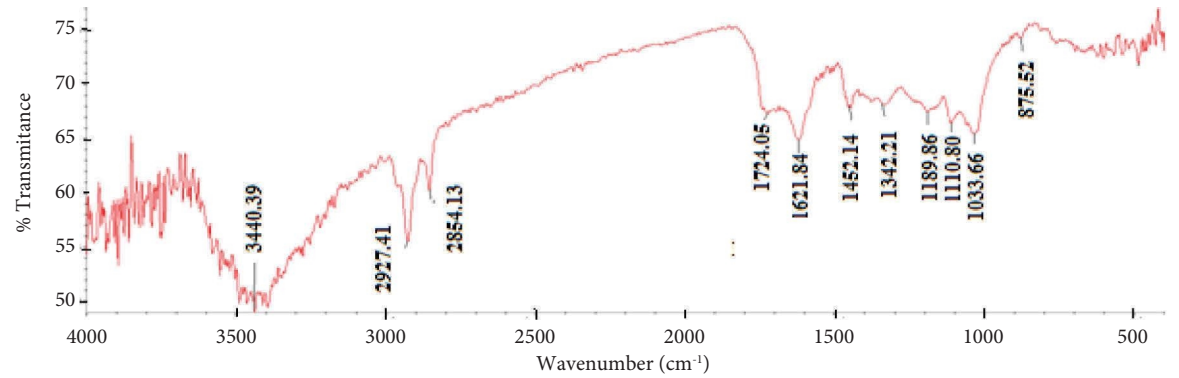

(a)

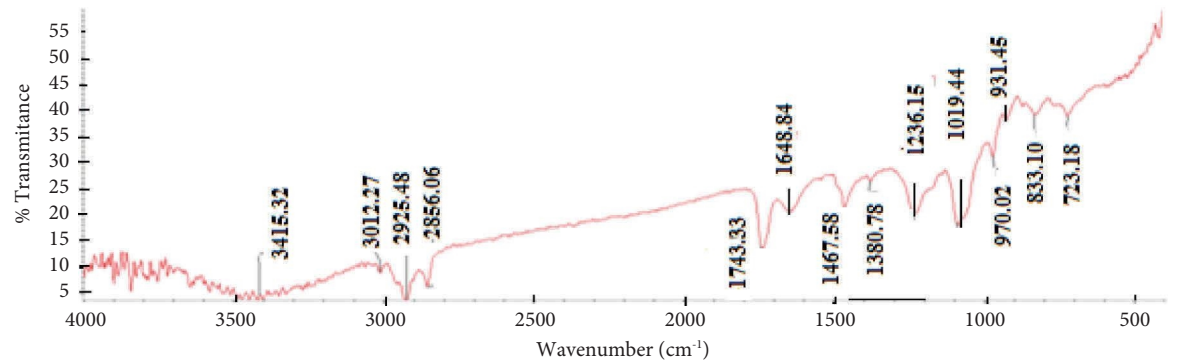

(b)

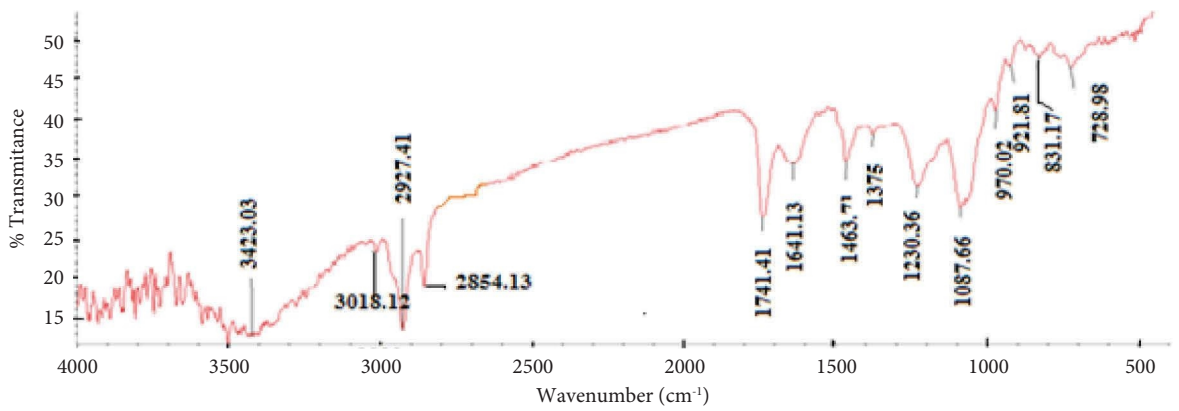

(c)

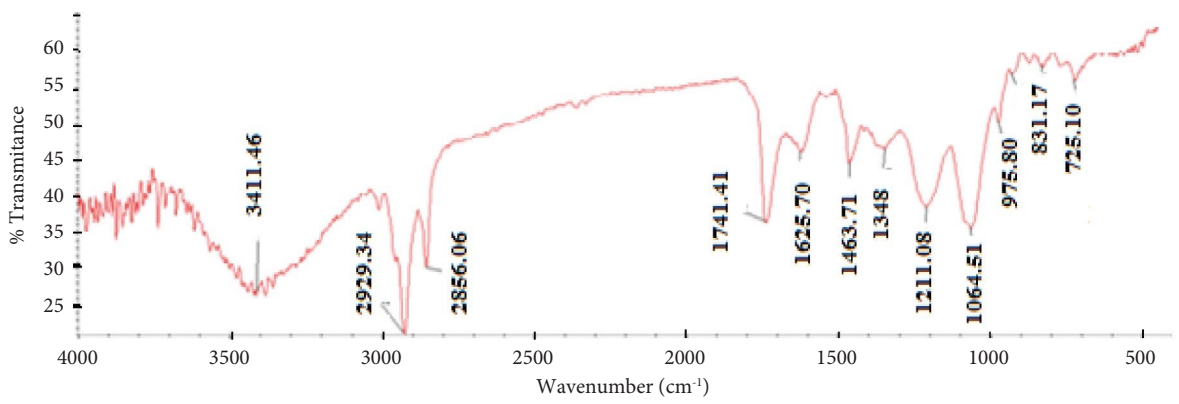

(d)

Figure 3: FTIR spectra of (a) EOE, (b) LECIVA S70, (c) PM, and (d) EOP.

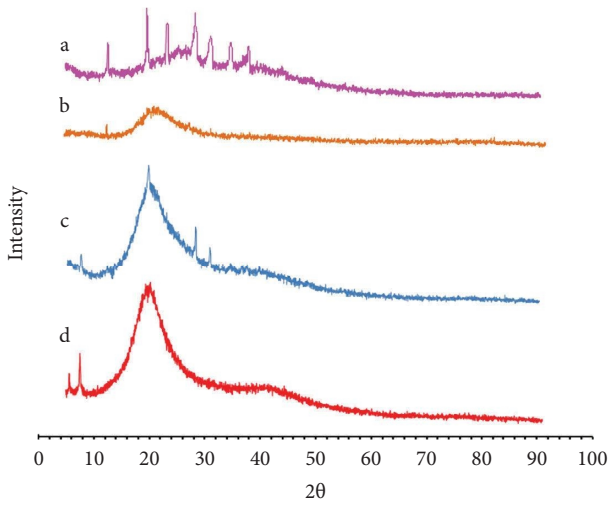

Figure 4: XRD overlay spectra of (a) EOE, (b) EOP, (c) PM, and (d) LECIVA S70.

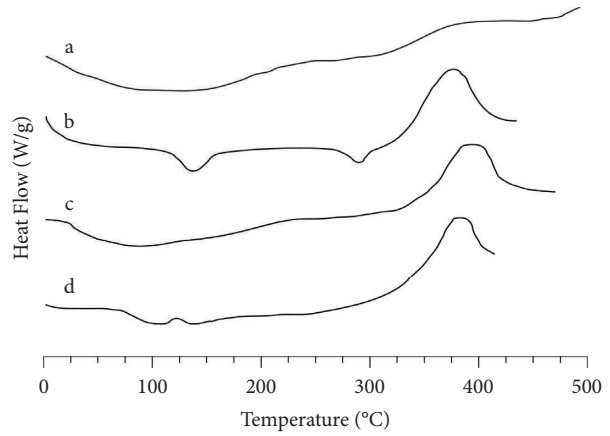

Figure 5: DSC thermogram: (a) EOE, (b) LECIVA S70, (c) EOP, and (d) PM.

33H at δ 3.756, 22H at δ 4.199, 21 H at δ 6.912, 2 H at δ 7.074, and 9 H at δ 7.377 in the ^{1}H NMR of EOE vanished in the ^{1}H NMR of EOP, indicating that hydrogen bonding was involved. Furthermore, 44 H at δ 1.232–1.255 in the ^{1}H NMR of LECIVA S70 appeared at δ 1.235–1.258 (35H) in the ^{1}H NMR of the EOP, indicating that phytosomes are formed. When the ^{1}H NMR graphs of EOP and LECIVA S70 were compared, it was discovered that proton signals in the LECIVA S70 shifted to the downfield with lower proton signal intensity. Because of the charge on phospholipids, intermolecular interactions between phospholipids and phytoconstituents are weak. The downfield chemical shift and lower intensity of proton signals confirmed the development of phytosomes.

3.9. Scanning Electron Microscopy (SEM). SEM photomicrograph of optimized EOP is shown in Figure 7. EOP formulation SEM photomicrographs were taken at 10.00 Kx magnifications and revealed the formation of multilayered vesicles of LECIVA S70 phospholipid. In addition, SEM photomicrographs found that the EOP formulation sample is semispherical and ovoid shaped, with encapsulated content shielded from the interior to the surface.

3.10. Solubility Analysis. The determining solubility of EOE, PM, and EOP in both water and octanol is shown in Table 4. The lipophilic character of EOE was demonstrated by its lower aqueous solubility ($11.85 \pm 0.25\,\mu$g/ml) and comparatively higher n-octanol solubility ($318.19 \pm 1.80\,\mu$g/ml). Compared to the EOE, the physical mixture (PM) had 1.59 times higher aqueous solubility but no significant difference in n-octanol solubility. On the other hand, EOP had a much higher aqueous solubility (7.58 times) than EOE ($p < 0.05$). The amphiphilic nature of the produced phytosomes (EOP) and the reduced molecular crystallinity or partial amorphization of the EOE can be attributed to a rise in the aqueous solubility of the EOE from the phytosomes [16, 30].

3.11. In Vitro Drug Release Studies. *In vitro* dissolution results of EOE, PM, and EOP are shown in Figure 8 and Supplementary Table 2. The release of EOE and PM was identical throughout the study period. Only roughly 21.33% of EOE was dissolved by the end of the dissolution period (i.e., up to 12 hours). In 12 hours, only about 33.35% of the PM was dissolved. The release profile of optimized phytosome formulation (EOP) was identical to that of EOE and PM for the first 20 minutes. Still, afterwards, the release of EOP rapidly increased, reaching $69.82 \pm 0.17\%$ at the end of 12 hours. At the end of the dissolving time, the obtained findings demonstrated a considerable release of EOE from the phytosomes. The optimized phytosome formulation followed a zero-order drug release kinetic model with a significance value of $p < 0.05$. EOE's higher wettability and solubility in the prepared phytosome may account for the considerable difference in the EOP release rate between EOE and PM. The following facts could explain this: (1) in the EOP, EOE transitions from a crystallized to a partially amorphous form, extending the pace and extent of breakdown to 12 hours, (2) improved solubility of EOE owing to the amphiphilic nature of LECIVA S 70, and (3) increased wettability and improved dispersion of EOP due to changes in the structural morphology of crystalline EOE into partial amorphization imparted due to the amphiphilic nature of LECIVA S 70 phospholipid [16, 31].

3.12. Stability Study. The stability study result of EOP is shown in Table 5. There was no discernible change in the EOP formulation during the prescribed storage duration. A slight drop in E.E. and increased *in vitro* drug release were detected throughout storage. This could be due to the medication being released from the lipid matrix. The temperature influences the lipid matrix over time, resulting in slender drug liberation from the interior and a modest increase in drug release. With extended storage periods, particles became larger, and zeta potential decreased. The phytosomes used in this research all had negative zeta

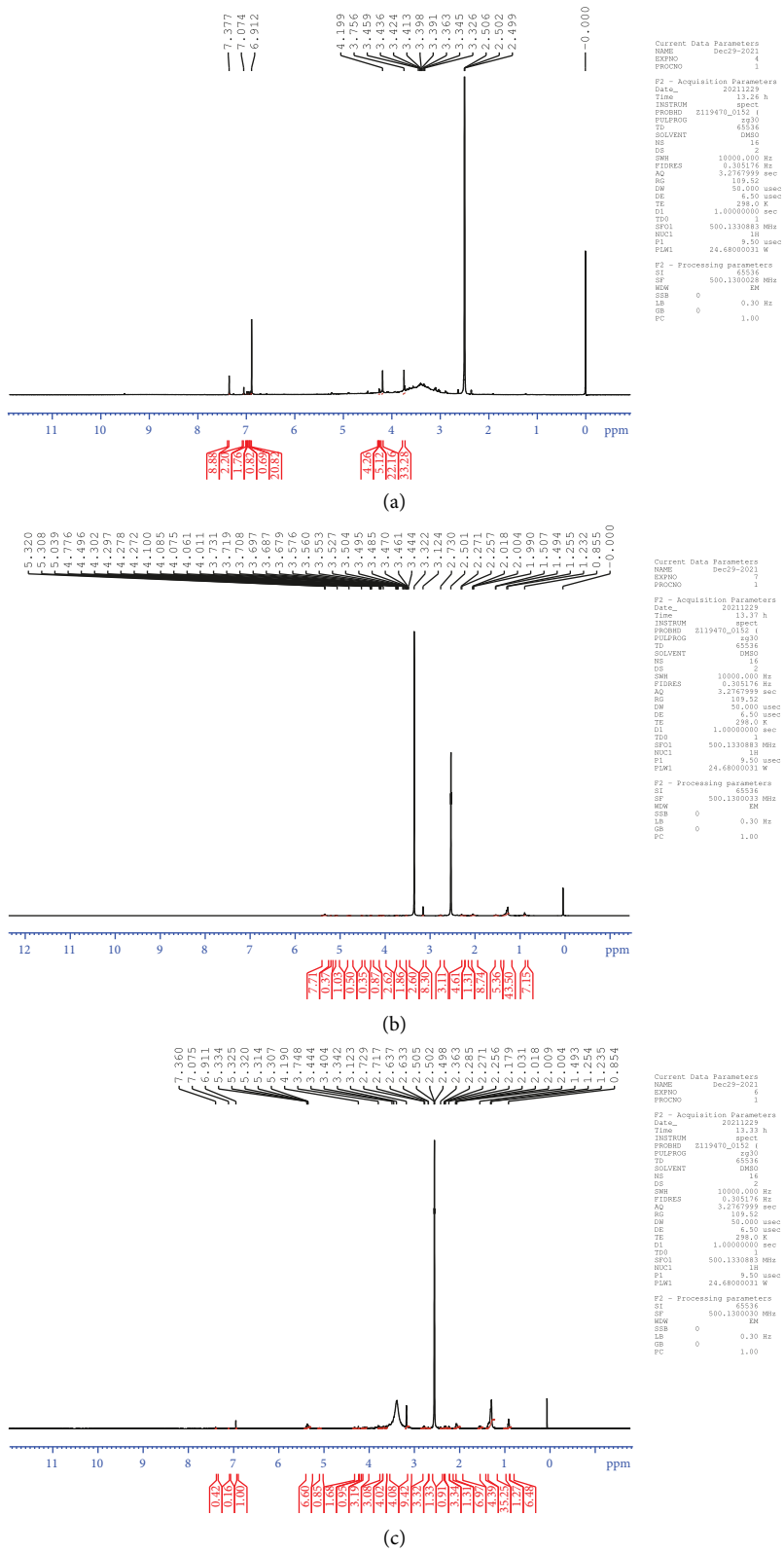

Figure 6: ^{1}H NMR of (a) EOE, (b) LECIVA S70, and (c) EOP.

potentials between −20 and −40 mV. Particles with identical electric charges may also cause repulsion. However, strong positive or negative zeta potential values can produce substantial repulsive forces, making redispersing the particles and avoiding clustering easy. A 20 mV or less zeta potential is optimal for a system with linked electrostatic and

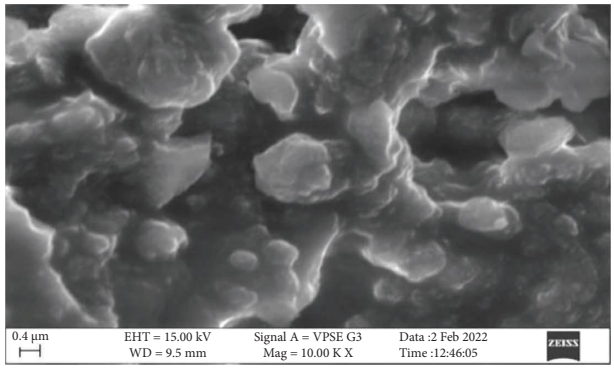

Figure 7: SEM photomicrograph of optimized EOP.

Table 4: Determined solubility of EOE, PM, and EOP.

Name of sample	Solubility (μg/ml)	
	Aqueous	n-octanol
EOE	11.85 ± 0.25	318.19 ± 1.80
PM	18.89 ± 0.20	332.75 ± 1.90
EOP	89.90 ± 0.24	340 ± 1.45

*The information is shown as mean ± SD values ($n = 3$).

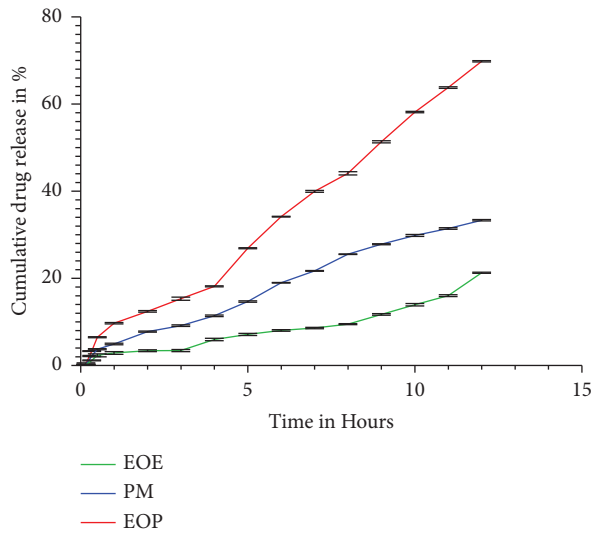

Figure 8: *In vitro* drug release of EOE, PM, and EOP (*the information is shown as mean ± SD values ($n = 3$)).

Table 5: Stability study result of EOP.

Parameters	Month		
	0	3	6
E.E. (%)	89.60 ± 0.7	87.24 ± 1.45	85.34 ± 0.55
In vitro drug release (%)	69.82 ± 0.17	72.45 ± 0.45	74.81 ± 0.29
Average particle size (nm)	198.4 ± 0.20	199.8 ± 0.15	204.2 ± 0.91
Zeta potential (mV)	−39.00 ± 0.40	−36.57 ± 1.30	−32.13 ± 1.70

*The information is shown as mean ± SD values ($n = 3$).

steric stabilization, while a high zeta potential (positive or negative) may provide physical stability. The entrapment efficiency data also suggested that the phytosomes kept the medications alive after six months. Six months of storage at varied temperatures and R.H. did not affect the formulation. Studies of the formulation's stability showed no change in size. Oral bioavailability can be greatly enhanced by decreasing particle size and increasing formulation stability. Smaller drug delivery systems are more effective. In conclusion, after six months in the temperature and humidity conditions of accelerated stability testing, the findings of all the investigations of entrapment efficiency, % drug release, particle size, and zeta potential claimed that phytosomes were in a satisfactory state of physical stability [17].

3.13. A Pharmacokinetic Study in the Blood Plasma Compartment. Once a single oral dose of EOE (250 mg/kg) and EOP (~250 mg/kg of EOE) has been administered, the mean plasma concentration-time profile and the HPLC chromatogram of standard gallic acid, EOE, and EOP in Wistar rat plasma are shown in Figure 9 and Supplementary Figure 2. The pharmacokinetic parameters were determined using P.K. Solver software and are shown in Table 6. According to the findings, C_{max}, T_{max}, and AUC 0-∞ in EOP-administered rats were considerably higher ($p < 0.05$) than in EOE-administered animals. EOP also had a longer half-life of absorption. In addition, the EOP-treated animals had a more extended residency and a longer duration of action than the EOE-treated animals, as evidenced by a lower CL/F and V/F ($p < 0.05$). The comparative bioavailability of the EOP was 2.71 times greater than that of the pure EOE. The enhancements in bioavailability in plasma after single oral dose administration of EOP are attributed to forming of molecular aggregates with amphiphilic phospholipid, improving aqueous solubility and enhancing intestinal absorption. Phospholipids are amphiphilic and can shield EOE from first-pass metabolism in the liver and increase bioavailability [16, 31].

3.14. In Vivo Memory-Enhancing Activity. We utilized one-way ANOVA and Tukey's multiple comparison tests to interpret the data. The first day's E.L./T.L. (on the 15th day of medication treatment) mirrored the development of animal learning behavior. On the other hand, animals' ability to retain information was reflected in the E.L./T.L. on day two or the 16th. A significant drop in E.L. and T.L. values validated memory improvement. Figure 10 depicts the findings of the *in vivo* memory-enhancing activity study.

3.14.1. Morris Water Maze Test. The animal's E.L., or how long it took to find the hidden platform, was quantified using MWMT. As shown in Figure 10(a), the E.L. of the scopolamine HBr-administered group increased significantly ($p < 0.05$) on day 16. On day 15, E.L. was substantially lower ($p < 0.0001$) in the piracetam and EOP + scopolamine HBr

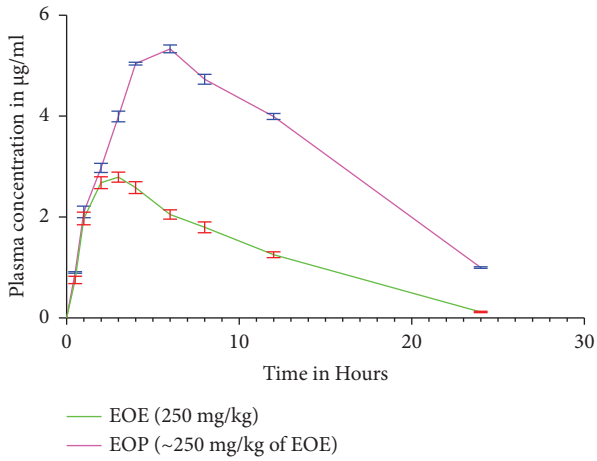

Figure 9: Mean plasma concentration-time profile after oral administration of EOE (250 mg/kg) and EOP (~250 mg/kg of EOE). The information is shown as mean ± SEM values ($n = 6$ in each group).

Table 6: Results of pharmacokinetic study after oral administration of EOE and EOP formulation.

Pharmacokinetic parameters	Treatment	
	EOE (250 mg/kg)	EOP (~250 mg/kg)
C_{max} (μg/ml)	2.72 ± 0.147	5.14 ± 0.164
T_{max} (h)	3.04 ± 0.004	6.1 ± 0.005
$AUC_{0\text{-}t}$ (μg/ml ∗ h)	29.91 ± 0.18	77.68 ± 0.15
$AUC_{0\text{-}\infty}$ (μg/ml ∗ h)	31.84 ± 0.11	86.42 ± 0.17
t1/2ka (h)	1.017 ± 0.22	4.08 ± 0.27
V/F (mg/kg)/(μg/ml)	125.48 ± 0.029	37.55 ± 0.035
CL/F (mg/kg)/(μg/ml)/h	15.70 ± 0.24	5.79 ± 0.17

*The information is shown as mean ± SD values ($n = 6$).

groups compared to the control group, and on day 16, E.L. was significantly lower ($p < 0.001$). It was also shown that the E.L. was similarly affected in the EOP + scopolamine HBr and piracetam groups. On days 15 and 16, E.L. was considerably lower in the piracetam, EOP + scopolamine HBr, and piracetam + scopolamine HBr groups than in the scopolamine HBr-administered group ($p < 0.0001$). In addition, compared to the EOE + scopolamine HBr group-, the EOP + scopolamine HBr-, and piracetam + scopolamine HBr-treated groups had significantly lower E.L. ($p < 0.01$) on the 15th day and ($p < 0.05$) on the 16th day. When compared to piracetam, the EOE + scopolamine HBr treatment group exhibited a substantial rise in E.L. ($p < 0.001$) on the 15th day and ($p < 0.05$) on the 16th day but a significant drop in E.L. ($p < 0.01$) compared to scopolamine HBr on both days and the vehicle control group ($p < 0.0001$ on the 15th day).

3.14.2. Elevated plus Maze Test. The length of time it took for a rat to hop on all fours from an open arm to covered arms housing the opposite sex was recorded (Figure 10(b)). On days 15 ($p < 0.05$) and 16 ($p < 0.001$), T.L. was substantially higher in the scopolamine HBr-treated group compared to the control group. Piracetam-, EOP + scopolamine HBr-, and piracetam + scopolamine HBr-treated groups exhibited significantly lower T.L. than control on days 15 ($p < 0.001$, $p < 0.001$, and $p < 0.01$) and 16 ($p < 0.001$, $p < 0.0001$, and $p < 0.001$). The T.L. was considerably ($p < 0.0001$) lower in the piracetam-, EOP + scopolamine HBr-, and piracetam + scopolamine HBr-treated groups compared to the scopolamine HBr-treated group on both days. The EOE + scopolamine HBr-administered Group had significantly ($p < 0.05$) higher T.L. than the Piracetam group and significantly ($p < 0.0001$) lower T.L. than the scopolamine HBr-treated Group. In addition, on days 15 ($p < 0.05$) and 16 ($p < 0.001$), T.L. was considerably lower in the EOP + scopolamine HBr group compared to the EOE + scopolamine HBr group.

In MWMT and EPMT, EOP exhibited higher efficiency than EOE. Administration of EOE, EOP, and piracetam for 15 consecutive days protected rat memory from memory impairment induced by the administration of scopolamine HBr. Hence, there was no observed significant increase in E.L./T.L. even after the administration of scopolamine HBr on the 16th day. As expected, piracetam was utilized as a positive control and showed considerable memory gains regarding E.L./T.L. The improved relative absorption of EOP following oral delivery may be due to enhanced relative absorption of EOE from EOP due to smaller particle size and interaction between phospholipid and EOE, which enhances the overall hydrophilicity and aqueous solubility of EOP. The phospholipid matrix in the EOP formulation may facilitate medication crossing and accommodation across the blood-brain barrier, which is important in memory improvement. As a result of the preceding observations, it is possible to conclude that in the MWMT and EPMT, the EOP + scopolamine HBr-administered group had a significantly lower E.L./T.L. than the EOE + scopolamine HBr-administered groups.

3.14.3. Acetylcholine Esterase Activity. EOE and EOP effects on brain Ach esterase activity in scopolamine HBr-induced Wistar rats are shown in Figure 11. Comparing the scopolamine HBr-treated group with the vehicle-treated control group, the scopolamine HBr group showed a statistically significant increase in Ach esterase activity ($p < 0.01$). As a result, the amount of the Ach transmitter in the body decreases as the active Ach esterase enzyme breaks down Ach. Compared to the vehicle-treated control group, Ach esterase activity was found to be significantly decreased ($p < 0.001$, $p < 0.01$, and $p < 0.01$) in the piracetam-, EOP + scopolamine HBr-, and piracetam + scopolamine HBr-treated groups, respectively. There was a statistically significant ($p < 0.0001$) rise in the Ach level at the cholinergic synapse in the piracetam, EOP + scopolamine HBr, piracetam + scopolamine HBr, and EOE + scopolamine HBr ($p < 0.001$) groups compared to the scopolamine HBr-given group. There was significantly decreased acetylcholine esterase activity ($p < 0.05$) in the EOP + scopolamine HBr-treated group compared with the EOE + scopolamine HBr-treated

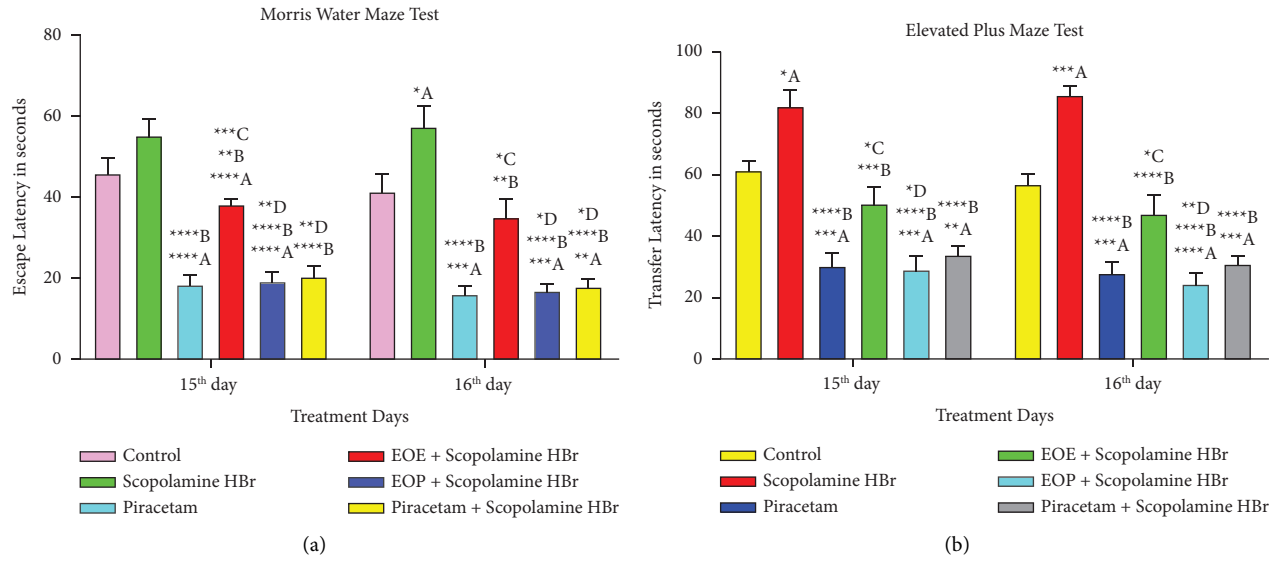

Figure 10: EOE and EOP affect spatial learning and memory in the (a) MWMT and (b) EPMT. The results are presented as mean ± SEM values ($n = 6$ in each group). A = compared to a vehicle-treated normal control group; B = compared to scopolamine HBr-treated group; C = compared with piracetam-treated group, and D = compared with EOE + scopolamine HBr-treated group ($^{*}p < 0.05$, $^{**}p < 0.01$, $^{***}p < 0.001$, and $^{****}p < 0.0001$) (one way ANOVA followed by Tukey's multiple comparisons test).

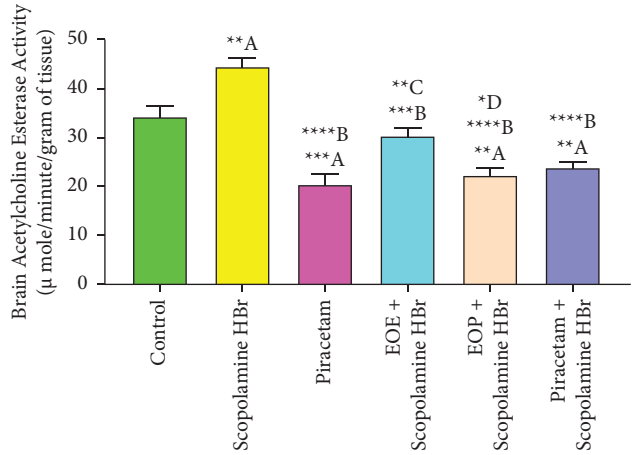

Figure 11: EOE and EOP effect on brain Ach esterase activity in scopolamine HBr-induced Wistar rats. The results are shown as mean ± SEM values ($n = 5$ in each group). A = compared to a vehicle-treated normal control group, B = compared to scopolamine HBr-treated group, C = compared with piracetam-treated group, and D = compared with EOE + scopolamine HBr-treated group ($^{*}p < 0.05$, $^{**}p < 0.01$, $^{***}p < 0.001$, and $^{****}p < 0.0001$) (one way ANOVA followed by Tukey's multiple comparisons test).

group. The significant suppression of Ach esterase activity following administering a dose of EOP similar to EOE extract (250 mg/kg) is largely attributable to the elevation of Ach levels. Numerous laboratory and clinical research studies have linked acetylcholine to cognitive control. That is why, by reducing AchE activity, EOP was more effective at raising Ach levels than EOE [32].

3.14.4. Estimation of Dopamine Concentration in Rat's Brain. Sandwich ELISA carried out the brain dopamine estimation, and a one-way ANOVA followed by Tukey's multiple comparison tests was used to evaluate dopamine levels. The brain dopamine concentration level is shown in Figure 12. The brain dopamine level was significantly increased ($p < 0.001$) in piracetam- and EOP + scopolamine HBr ($p < 0.01$)-treated groups compared to the control group. There was also a significant increase in the brain dopamine level in the piracetam ($p < 0.0001$), EOE + scopolamine HBr ($p < 0.05$), EOP + scopolamine HBr ($p < 0.0001$), and piracetam + scopolamine HBr ($p < 0.05$) treated groups compared to the scopolamine HBr group. Brain dopamine levels were considerably ($p < 0.05$) higher in the EOP-treated group than in the EOE. The brain dopamine concentration was 16.27 ± 1.209 and 10.40 ± 1.185 ng/ml in the EOP and pure extract-treated groups, respectively. The amphiphilic nature of phospholipids and the formation of smaller particles may

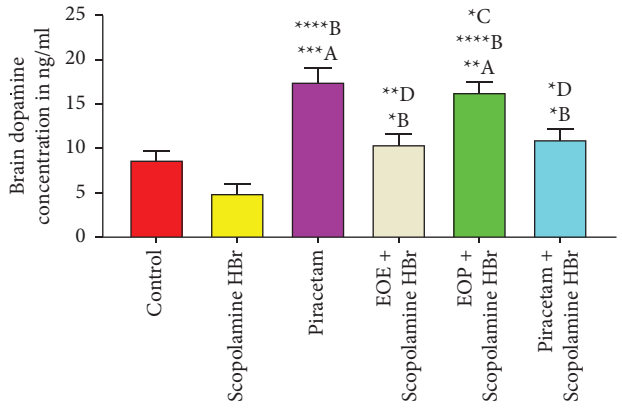

Figure 12: Brain dopamine concentration level. Data are expressed as mean ± SEM values ($n = 5$ in each group). A = compared to a vehicle-treated normal control group; B = compared to the scopolamine HBr-treated group; C = compared with EOE + scopolamine HBr-treated group, and D = compared to the piracetam-treated group ($^{*}p < 0.05$, $^{**}p < 0.01$, $^{***}p < 0.001$, and $^{****}p < 0.0001$) (one-way ANOVA followed by Tukey's multiple comparisons test).

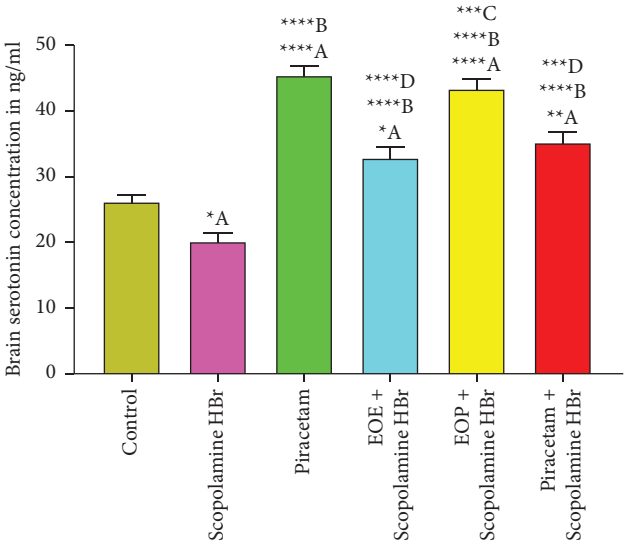

Figure 13: Brain serotonin concentration level. Data are expressed as mean ± SEM values ($n = 5$ in each group). A = compared to a vehicle-treated normal control group; B = compared to the scopolamine HBr-treated group; C = compared with EOE + scopolamine HBr-treated group, and D = compared to the piracetam-treated group ($^{*}p < 0.05$, $^{**}p < 0.01$, $^{***}p < 0.001$, and $^{****}p < 0.0001$) (one-way ANOVA followed by Tukey's multiple comparisons test).

be responsible for increasing the EOP concentration in the brain, which in turn affects the dopaminergic pathway and increases dopamine concentration in the rat brain. The release of dopamine acts on the dopamine receptor in the brain and neurons and shows the effects of dopamine, such as movement, coordination, pleasure, and cognition. The prepared phytosome formulation (EOP) significantly protects memory from scopolamine-induced memory impairment and enhances cognitive function by increasing dopamine concentration. Impairment of cognitive, behavioral, and fine motor abilities might result from decreased DA concentration or suppression of its production or metabolism rates in the central nervous system [33–35].

3.14.5. Estimation of Serotonin Concentration in Rat Brain. The sandwich ELISA technique was used for the estimation of brain serotonin levels. The result is exhibited in Figure 13. A one-way ANOVA followed by Tukey's multiple comparison tests was used to evaluate serotonin levels. The brain serotonin level was significantly increased in piracetam ($p < 0.0001$), EOE + scopolamine HBr ($p < 0.05$), EOP + scopolamine HBr ($p < 0.0001$), and piracetam + scopolamine HBr ($p < 0.01$) and significantly reduced in scopolamine HBr ($p < 0.05$) when compared to the control group. The level of serotonin was found to be very low in the scopolamine HBr-treated group, which was used for inducing amnesia. The brain serotonin level was significantly increased ($p < 0.0001$) in all the treatment groups except the control group compared to the scopolamine-treated group. There has been a significant increase in brain serotonin ($p < 0.001$) in the EOP formulation-treated group as compared to EOE + scopolamine HBr, and it may be due to an increase in the concentration of EOP in the brain, which may be positively affecting the serotonergic pathway. When compared with the piracetam-treated group (positive control), the serotonin level was found to be significantly decreased in EOE + Scopolamine HBr ($p < 0.0001$) and piracetam + scopolamine HBr ($p < 0.001$). An increased level of brain serotonin was observed in the EOP formulation-treated group (43.28 ± 1.550 ng/ml) compared to the pure extract (32.79 ± 1.738 ng/ml).

Pathological alterations in the cholinergic, glutamatergic, serotonergic, and noradrenergic transmitter systems have been linked to cognitive function and memory impairment in patients with neurodegenerative diseases. These results suggest that several neurotransmitters play a role in memory development and retrieval. Rats' cognitive abilities are evaluated by measuring perception, attention, drive, emotion, and movement. There is some evidence that serotonergic activity plays a pivotal role in tasks that involve dealing with feelings. One of the most crucial neurotransmitters for learning and memory is serotonin, synthesized from the amino acid tryptophan. Parts of the brain involved in learning and memory contain 5-HT pathways, 5-HT reuptake site/transporter (SERT), and 5-HT receptors. Ascending raphe nuclei in the brain stem are the site of serotonin (5-HT) synthesis, storage, and reuptake, and their serotonergic projections reach nearly all forebrain regions involved in learning and memory. 5-HT influences the transmission of information via cholinergic and glutamatergic pathways. Memory was negatively affected by low serotonin levels in the brain. In this study, we observed an improvement in memory and learning and an increase in serotonin levels in the EOP-treated group compared to the pure extract [35–37].

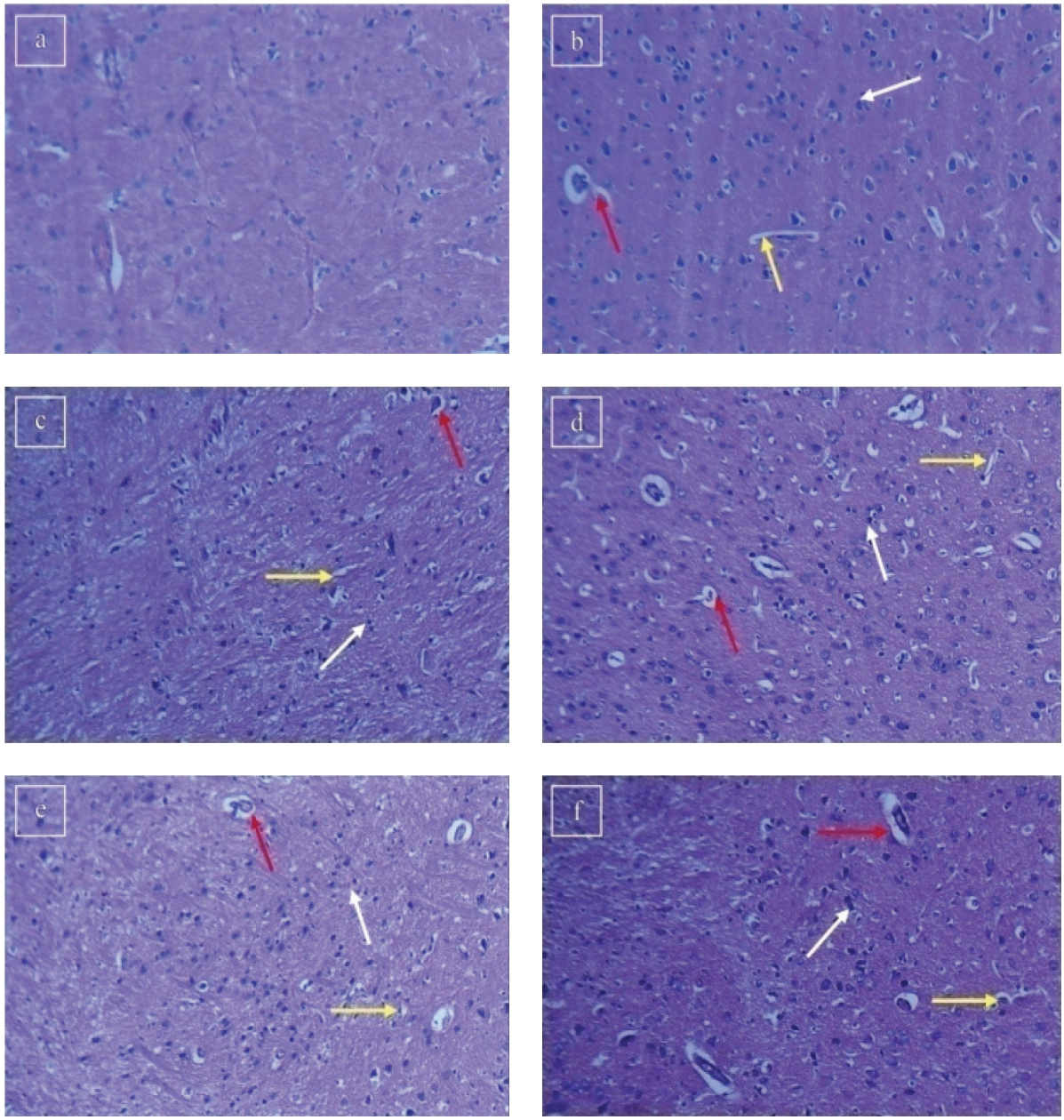

Figure 14: Histopathological study micrographs of rat brain: (a) Group I, (b) Group II, (c) Group III, (d) Group IV, (e) Group V, and (f) Group VI. Yellow, white, and red-collared arrow indicates vascular degeneration, glial cell infiltration, and neuronal degeneration, respectively.

3.15. Estimation of the Concentration of EOE and EOP in Brain Tissue. Gallic acid concentrations in brain tissue measured following EOP oral administration ($1.06 \pm 0.04\,\mu$g/ml) were substantially greater ($p < 0.05$) than EOE ($0.32 \pm 0.07\,\mu$g/ml). This confirms the enhanced brain delivery of EOE by phytosome (EOP). This could be due to phospholipid's presence in phytosomes, which could have resulted in changes in G.I. tract permeability and blockage of an apically polarized efflux mechanism and smaller particle size.

3.16. Histopathological Study. The findings of the histopathological investigation of the brain are displayed in Figure 14. Group I (the normal control group) did not exhibit any toxicity in terms of neuronal, vascular degeneration, or glial cell infiltration (Figure 14(a)). The brain of the disease-control animal showed moderate vascular and cerebral neuronal degeneration, necrosis, and glial cell infiltration (Figure 14(b)). However, other animals belonging to other treatment groups showed mild pathological changes compared to disease control. Mild types of glial cell

infiltration and neuronal and vascular degeneration were observed in the piracetam (Figure 14(c)), EOE (Figure 14(d)), and piracetam + scopolamine HBr (Figure 14(f)) administered groups. Compared to the EOE-treated group, the EOP-treated animals' brains exhibited much less neuronal and vascular degeneration and glial cell infiltration (Figure 14(e)) [21, 32, 38].

4. Conclusions

In this investigation, a complex with phospholipid was formed into a phytosome to increase the aqueous solubility, permeability, bioavailability, and memory-enhancing action of EOE. The developed phytosomal formulation of EOE was optimized using the Box-Behnken design, which showed improved solubility and *in vivo* memory enhancement in rats. Phytosomal preparations exhibited higher efficacy in MWMT and EPMT than EOE. The histopathological finding revealed the presence of mild toxicity as compared to the EOE-treated group. Furthermore, EOP exhibited 2.7-fold greater bioavailability than plain EOE. When compared to EOE, the higher concentration of EOP in brain tissue may have resulted from the formation of particles smaller than 200 nm. Finally, using phytosomes as a drug delivery mechanism improves EOE solubility and, as a result, exhibits memory-enhancing potential in rats. The amphiphilic nature of phospholipids could lead to the formation of a homogenous amorphous matrix of EOE in the lipid bilayer, which further results in an increase in solubility and bioavailability. This is attributable to AchE inhibitory activity. The increase in acetylcholine, dopamine, and serotonin neurotransmitter levels may be attributed to the enhancement of the nootropic potential of EOP as compared to EOE.

Data Availability

The data used to support the findings of this study are available from the corresponding author upon request.

Conflicts of Interest

The authors declare that they have no conflicts of interest.

Acknowledgments

The authors would like to extend their appreciation to Arjuna Remedies, Kerala, who generously sent a sample of their *Emblica officinalis* extract. Finally, ChromeIn, Pune Chromatographic Technology and Services, is acknowledged for their assistance with HPLC analysis. This study was self-funded.

Supplementary Materials

Supplementary file contains two additional figures as well as tables supporting the results of the study. (*Supplementary Materials*)

References

[1] K. M. Kantak, "Corrigendum to Adolescent-onset vs. adult-onset cocaine use: impact on cognitive functioning in animal models and opportunities for translation," *Pharmacology Biochemistry and Behavior*, vol. 206, Article ID 173191, 2021.

[2] S. D. Saoji, N. A. Raut, P. W. Dhore, C. D. Borkar, M. Popielarczyk, and V. S. Dave, "Preparation and evaluation of phospholipid-based complex of standardized Centella extract (SCE) for the enhanced delivery of phytoconstituents," *The AAPS Journal*, vol. 18, no. 1, pp. 102–114, 2015.

[3] G. Logroscino, B. P. Imbimbo, M. Lozupone et al., "Promising therapies for the treatment of frontotemporal dementia clinical phenotypes: from symptomatic to disease-modifying drugs," *Expert Opinion on Pharmacotherapy*, vol. 20, no. 9, pp. 1091–1107, 2019.

[4] G. Karthivashan, P. Ganesan, S. Y. Park, J. S. Kim, and D. K. Choi, "Therapeutic strategies and nano-drug delivery applications in management of ageing Alzheimer's disease," *Drug Delivery*, vol. 25, no. 1, pp. 307–320, 2018.

[5] W. Wilms, M. Woźniak-Karczewska, P. F. X. Corvini, and Ł Chrzanowski, "Nootropic drugs: methylphenidate, modafinil and piracetam – population use trends, occurrence in the environment, ecotoxicity and removal methods – a review," *Chemosphere*, vol. 233, pp. 771–785, 2019.

[6] B. C. Variya, A. K. Bakrania, and S. S. Patel, "Emblica officinalis (Amla): a review for its phytochemistry, ethnomedicinal uses and medicinal potentials with respect to molecular mechanisms," *Pharmacological Research*, vol. 111, pp. 180–200, 2016.

[7] J. Hüsch, J. Bohnet, G. Fricker et al., "Enhanced absorption of boswellic acids by a lecithin delivery form (Phytosome®) of Boswellia extract," *Fitoterapia*, vol. 84, pp. 89–98, 2013.

[8] J. Khan, A. Alexander, S. S. Ajazuddin, S. Saraf, and S. Saraf, "Recent advances and future prospects of phyto-phospholipid complexation technique for improving pharmacokinetic profile of plant actives," *Journal of Controlled Release*, vol. 168, no. 1, pp. 50–60, 2013.

[9] K. Mukherjee, M. Venkatesh, P. Venkatesh, B. P. Saha, and P. K. Mukherjee, "Effect of soy phosphatidyl choline on the bioavailability and nutritional health benefits of resveratrol," *Food Research International*, vol. 44, no. 4, pp. 1088–1093, 2011.

[10] S. M. A. Zaidi, S. A. Pathan, F. J. Ahmad, S. Surender, S. Jamil, and R. K. Khar, "Neuropharmacological evaluation of *Paeonia emodi* root extract phospholipid complex in mice," *Planta Medica*, vol. 77, no. 05, p. 123, 2011.

[11] S. Rathee and A. Kamboj, "Optimization and development of antidiabetic phytosomes by the Box-Behnken design," *Journal of Liposome Research*, vol. 28, no. 2, pp. 161–172, 2017.

[12] S. Ahalwat, D. C. Bhatt, and S. Rohilla, "Quality by design (QbD) based formulation optimization of isoniazid loaded novel nanostructured lipid carriers for controlled release effect," *Journal of Pharmaceutical Innovation*, vol. 18, no. 4, pp. 1685–1700, 2023.

[13] P. Mohit Kumar, P. Kumar, P. Solanki, B. Mangla, and G. Aggarwal, "Formulation development, optimization by box-behnken design, and in vitro characterization of gefitinib phospholipid complex based nanoemulsion drug delivery system," *Journal of Pharmaceutical Innovation*, vol. 18, no. 3, pp. 952–964, 2022.

[14] J. Zhang, Q. Tang, X. Xu, and N. Li, "Development and evaluation of a novel phytosome-loaded chitosan microsphere system for curcumin delivery," *International Journal of Pharmaceutics*, vol. 448, no. 1, pp. 168–174, 2013.

[15] A. Sze, D. Erickson, L. Ren, and D. Li, "Zeta-potential measurement using the dmoluchowski equation and the slope of the current time relationship in electro osmotic flow," *Journal of Colloid and Interface Science*, vol. 261, pp. 402–410, 2003.

[16] D. R. Telange, A. T. Patil, A. M. Pethe, H. Fegade, S. Anand, and V. S. Dave, "Formulation and characterization of an apigenin-phospholipid phytosome (APLC) for improved solubility, in vivo bioavailability, and antioxidant potential," *European Journal of Pharmaceutical Sciences*, vol. 108, pp. 36–49, 2017.

[17] S. S. Salunkhe, N. M. Bhatia, and M. S. Bhatia, "Implications of formulation design on lipid-based nanostructured carrier system for drug delivery to brain," *Drug Delivery*, vol. 23, no. 4, pp. 1306–1316, 2014.

[18] B. Ceylan, E. K. Tekkeli, and C. Önal, "Development of an HPLC method for the determination of mesalazine in human plasma by fluorimetric derivatization and application to a prototype pharmacokinetic study," *Journal of Fluorescence*, vol. 32, no. 1, pp. 319–325, 2021.

[19] D. J. Kalal and V. K. Redasani, "Stability-indicating RP-HPLC method development and validation for estimation of Mupirocin calcium in bulk and in pharmaceutical formulation," *Future Journal of Pharmaceutical Sciences*, vol. 8, no. 1, p. 21, 2022.

[20] T. Yaguchi, T. Nagata, and T. Nishizaki, "Corrigendum to 1-Palmitoyl-2-oleoyl-sn-glycero-3-phosphocholine improves cognitive decline by enhancing long-term depression," *Behavioural Brain Research*, vol. 204, pp. 129–132, 2016.

[21] G. M. Abdelwahab, A. Mira, Y. B. Cheng, T. A. Abdelaziz, M. F. I. Lahloub, and A. T. Khalil, "Acetylcholine esterase inhibitory activity of green synthesized nanosilver by naphthopyrones isolated from marine-derived *Aspergillus niger*," *PLoS One*, vol. 16, no. 9, Article ID e0257071, 2021.

[22] P. K. Gaur, D. Puri, A. P. Singh, N. Kumar, and S. Rastogi, "Optimization and pharmacokinetic study of boswellic acid–loaded chitosan-guggul gum nanoparticles using Box-Behnken experimental design," *Journal of Pharmaceutical Innovation*, vol. 17, no. 2, pp. 485–500, 2021.

[23] A. Ahmad, M. U. Rehman, A. F. Wali et al., "Box-Behnken response surface design of polysaccharide extraction from *Rhododendron arboreum* and the evaluation of its antioxidant potential," *Molecules*, vol. 25, no. 17, p. 3835, 2020.

[24] M. Danaei, M. Dehghankhold, S. Ataei et al., "Impact of particle size and polydispersity index on the clinical applications of lipidic nanocarrier systems," *Pharmaceutics*, vol. 10, no. 2, p. 57, 2018.

[25] A. Zafar, N. K. Alruwaili, S. S. Imam et al., "Development and optimization of nanolipid-based formulation of diclofenac sodium: in vitro characterization and preclinical evaluation," *Pharmaceutics*, vol. 14, no. 3, p. 507, 2022.

[26] D. R. Telange, N. K. Sohail, A. T. Hemke, P. S. Kharkar, and A. M. Pethe, "Phospholipid complex-loaded self-assembled phytosomal soft nanoparticles: evidence of enhanced solubility, dissolution rate, ex vivo permeability, oral bioavailability, and antioxidant potential of mangiferin," *Drug Delivery and Translational Research*, vol. 11, no. 3, pp. 1056–1083, 2020.

[27] S. K. Jena, C. Singh, C. P. Dora, and S. Suresh, "Development of tamoxifen-phospholipid complex: novel approach for improving solubility and bioavailability," *International Journal of Pharmaceutics*, vol. 473, no. 1-2, pp. 1–9, 2014.

[28] M. Sukmawaty, A. D. Permana, A. D. Permana, M. Mudjahid, T. P. Roska, and L. Rahman, "Lipid complex-itraconazole in thermosensitive mucoadhesive vaginal gel to enhance the effectiveness of therapy for vulvovaginal candidiasis: formulation, optimization, characterization, and ex vivo evaluation," *Journal of Pharmaceutical Innovation*, vol. 18, no. 3, pp. 1546–1559, 2023.

[29] X. Yanyu, S. Yunmei, C. Zhipeng, and P. Qi-Neng, "The preparation of silybin–phospholipid complex and the study on its pharmacokinetics in rats," *International Journal of Pharmaceutics*, vol. 307, no. 1, pp. 77–82, 2005.

[30] M. Wang, S. K. You, H. K. Lee et al., "Development and evaluation of docetaxel-phospholipid complex loaded self-microemulsifying drug delivery system: optimization and in vitro/ex vivo studies," *Pharmaceutics*, vol. 12, no. 6, p. 544, 2020.

[31] S. Rathor and D. C. Bhatt, "Formulation, characterization, and pharmacokinetic evaluation of novel glipizide-phospholipid nano-complexes with improved solubility and bioavailability," *Pharmaceutical Nanotechnology*, vol. 10, no. 2, pp. 125–136, 2022.

[32] S. Shayesteh, M. Khalilzadeh, N. Takzaree, and A. R. Dehpour, "Dapsone improves the vincristine-induced neuropathic nociception by modulating neuroinflammation and oxidative stress," *Daru Journal of Pharmaceutical Sciences*, vol. 30, no. 2, pp. 303–310, 2022.

[33] C. Gopi, V. G. Sastry, and M. D. Dhanaraju, "Effect of novel phenothiazine derivatives on brain dopamine in Wistar rats," *Beni-Suef University Journal of Basic and Applied Sciences*, vol. 8, no. 1, p. 7, 2019.

[34] M. V. Puig, J. Rose, R. Schmidt, and N. Freund, "Dopamine modulation of learning and memory in the prefrontal cortex: insights from studies in primates, rodents, and birds," *Frontiers in Neural Circuits*, vol. 8, p. 93, 2014.

[35] T. Myhrer, "Neurotransmitter systems involved in learning and memory in the rat: a meta-analysis based on studies of four behavioral tasks," *Brain Research Reviews*, vol. 41, no. 2–3, pp. 268–287, 2003.

[36] S. S. Mateos, C. L. Sánchez, S. D. Paredes, C. Barriga, and A. B. Rodríguez, "Circadian levels of serotonin in plasma and brain after oral administration of tryptophan in rats," *Basic and Clinical Pharmacology and Toxicology*, vol. 104, no. 1, pp. 52–59, 2009.

[37] A. Meneses and G. Liy-Salmeron, "Serotonin and emotion, learning and memory," *Reviews in the Neurosciences*, vol. 23, no. 5–6, pp. 543–553, 2012.

[38] A. Kumar, S. Dogra, and A. Prakash, "Neuroprotective effects of *Centella asiatica* against intracerebroventricular colchicine-induced cognitive impairment and oxidative stress," *International Journal of Alzheimer's Disease*, vol. 2009, pp. 1–8, 2009.